



Systematic design methodology for development and flight testing of a variable pitch quadrotor biplane VTOL UAV for payload delivery[☆]

Vishnu S. Chipade, Abhishek*, Mangal Kothari, Rushikesh R. Chaudhari

Department of Aerospace Engineering Indian Institute of Technology Kanpur, Kanpur, UP, 208016 India



ARTICLE INFO

Keywords:

Variable pitch
Quadrotor tailsitter UAV
UAV design
Blade element theory
Payload delivery

ABSTRACT

This paper discusses the conceptual design and proof-of-concept flight demonstration of a novel variable pitch quadrotor biplane Unmanned Aerial Vehicle concept for payload delivery. The proposed design combines vertical take-off and landing (VTOL), precise hover capabilities of a quadrotor helicopter and high range, endurance and high forward cruise speed characteristics of a fixed wing aircraft. The proposed methodology is described by taking an example of a VTOL Unmanned Aerial Vehicle (UAV) for a mission requirement of carrying and delivering 6 kg payload to a destination at 16 km from the point of origin. First, the design of propellers is carried out using a physics based modified Blade Element Momentum Theory (BEMT) analysis, which is validated using experimental data generated for the purpose. Propellers have conflicting requirement for optimal hover and forward flight performance and a compromise solution has to be chosen. Next, the biplane wings are designed using simple lifting line theory. The airframe design is followed by power plant selection and transmission design. Finally, weight estimation is carried out to complete the design process. The propeller design with 24° preset angle and -24° twist is found to be suitable for the current mission profile, based on 70% weightage to forward flight and 30% weightage to hovering flight conditions. A reduction in operating RPM of the propellers from 3200 during hover to 2000 during forward flight results in 27% increase in propeller efficiency. The VTOL UAV design proposed in this paper is also predicted to consume 64% less power in airplane mode compared to the quadrotor mode, thereby establishing the benefit of this hybrid concept. A proof-of-concept scaled prototype is fabricated using commercial-off-the-shelf parts and a Proportional Integral Derivative (PID) controller is developed and implemented on open source PixHawk autopilot board to enable stable hovering flight and attitude tracking during hover flight tests.

1. Introduction

With increased popularity of internet shopping, e-commerce sector faces a daunting task of delivering huge volumes of packages on time. The technological revolution in the area of Unmanned Aerial System has provided the sector a plausible solution that can not only deliver the packages on time but also to remote areas with difficult terrains. Amazon, Google, Alibaba and other e-commerce giants are already working on developing their own Unmanned Aerial Vehicle (UAV) solutions with small payload capacity to cater to the “last mile”, as it can augment their profit by cutting labor cost. Apart from e-commerce sector, emergency health-care sector is also showing tremendous interest in UAVs with automatic payload delivery system, which can be used to deliver life saving drugs or blood over remote areas. Autonomous payload delivery requires the UAV to do precise hover at low altitude above ground and fly long distances efficiently, both of which have conflicting requirements. The rotary wing UAVs offer the ability to hover and vertical take-off and

landing (VTOL), but are known to have less efficiency and speed than the fixed wing UAVs. Fixed wing UAVs have been used widely because of their simple design, high endurance, high range and high speed capability, but these are incapable of VTOL. Therefore, there is a need for hybrid design of UAVs that combine VTOL capabilities with high speed, range and endurance.

The common hybrid VTOL concepts studied in literature include monoplane wing tail-sitter [1,2], tiltrotor [3–5], compound helicopter [6], quad tiltrotor [7], quad-tiltwing [8] concepts. The monoplane tail sitter concept has the simplest design, but suffers from poor control authority during hover due to use of one propeller. The transition from hover to forward flight and back is quite challenging in these vehicles. Mimicking the V-22 Osprey tiltrotor design in small sized UAVs is cumbersome as it requires use of swashplate for controlling the pitch angle of each of the rotors making it mechanically complicated and therefore is only suitable for larger sized UAVs, for example none of [3–5], which are small scale variants, use swashplate. The fixed pitch

* This paper was recommended for publication by associate editor Dr. Y.-Q. Chen.

* Corresponding author.

E-mail address: abhis@iitk.ac.in (Abhishek).

Nomenclature

A	Rotor disk area
$\mathcal{R}, \mathcal{R}_{wt}$	Aspect ratio of rotor and wing respectively
a_p, d_t	Addendum and dedendum of gear respectively
b_t	Gear face width
b_w	Span of the wing
B	Bevel gear
c, c_w	Chord of the rotor and wing respectively
C_b, C_d	2D Coefficient of lift and drag respectively
C_{D_0}	Parasitic drag coefficient of the wing
$C_{L_{cr}}, C_{L_{max}}$	Lift coefficient during cruise and maximum lift coefficient
C_T, C_P	Coefficient of thrust and power respectively
C_{Th}	Coefficient of thrust during hover
D	Drag
E	Engine gear
E, E_d	Vector representing actual Euler angles and desired Euler angles respectively
e_a, e_p	Error vector for Euler angles and position respectively
F	Prandtl's tip loss factor
FM	Figure of merit
F_t	Load transmitted by gears
g	Acceleration due to gravity
K	Induced drag factor
K_f, K_m	Factor for stress concentration effect and load distribution respectively
K_F	Rotor force constant
K_p^a, K_i^a, K_d^a	PID gains for attitude control
K_p^p, K_i^p, K_d^p	PID gains for position control
K_o, K_v	Factor for loading and dynamic loading respectively
l, m, n	Total Moments about body fixed x, y, z axes
L	Lift
M	Mass of the vehicle
M	Vector of moments acting on the vehicle
$M1, M2$	Middle gears
N_b	Number of blades
P, P_{ind}	Total power and induced power respectively
P_d	Pitch circle diameter
PL	Power loading
r	Non-dimensional radial position, $= y/R$
r, r_d	Actual position and desired position vector of the vehicle
R	Rotor blade radius
$S1, S2$	Shaft gears
S_w	Wing area
T	Thrust
T_1, T_2	Gear teeth ratio for gear 1 and 2
TR	Taper ratio
u_i, w_i	Induced swirl and axial velocity respectively
U_T, U_P	Sectional in plane and out of plane velocity respectively
U	Resultant Velocity
v_i	Resultant induced velocity
$V_\infty, V_{cr}, V_{stall}$	Free stream velocity, cruise velocity and stall velocity respectively
W	Weight
(x, y, z)	Position of the vehicle
(x_d, y_d, z_d)	Desired position of the vehicle
y_r	Distance along blade from rotational axis
Y	Lewis factor
α	Angle of attack

β	Ratio of span of biplane to that of monoplane
γ	$\tan^{-1}(C_d/C_l)$
η_p	Propeller efficiency
θ	Blade pitch angle
λ, λ_i	Out of plane velocity ratio and induced velocity ratio respectively
μ	Advance ratio
ξ, ξ_i	In plane velocity ratio and induced velocity ratio respectively
ρ	Air density
σ	Solidity $= \frac{N_b c}{\pi R}$
σ_b	Maximum bending stress
Φ	Inflow angle
(ϕ, θ, ψ)	Euler angle representing attitude of the quadrotor
$(\phi_d, \theta_d, \psi_d)$	Desired Euler angle representing desired attitude of the quadrotor
ϕ_0	Pressure angle for gear
Ω	Rotor angular velocity (rad/sec)
AGMA	American Gear Manufacturers Association
VTOL	Vertical Take-off Landing
UAV	Unmanned Aerial Vehicle

propeller based designs as that of [3] are easy to build but suffer from poor stability and control authority in pitch mode. Lift and thrust compounding results in **high empty weight** and therefore has not been attempted in 1–2 kg class small UAVs. The quad tiltrotor design has good control authority during hover and transition and its flight control is simpler than that for monoplane tail-sitter. But, the rotor wing interaction in hover and the aerodynamic interaction between fore and aft wings result in loss of efficiency. The interaction losses during hover for quad tiltrotor is addressed in the quad-tiltwing design of Cetinsoy et al. [8]. It has four rotors that are mounted on the four wings. The wings, together with the rotors, are tilted between vertical and horizontal configurations to accomplish vertical and horizontal flights. It hovers like a quadrotor and flies like a tandem wing airplane in forward flight mode. However, the transition from hover to forward flight and back to hover offers significant challenges due to the flow separation on the wing operating at very angle of attack at the beginning of the transition. The convertiplane design of Abhishek et al. [9] offers a better compromise with part of the wing under the downwash of rotor tilting with it to eliminate hover losses. Also, since significant portion of the wing remains straight and facilitates transition.

Google X, a division of Google, developed and carried out field trials of a tailsitter aircraft with four fixed pitch propellers offset from the wing [10] to enable smooth transition from hover to forward flight and back, which after extensive testing was deemed unsuitable at maintaining its attitude during windy conditions due to lack of control power. The four propellers were quite close to each other and therefore were unable to generate adequate control moments. Amazon's solution for Amazon Prime Air package delivery UAV prototype [11] is a battery driven vehicle with four sets of coaxial contra-rotating propellers for vertical takeoff, hover and landing and tandem wings with pusher propeller for forward flight. The four coaxial propellers operate like that of a **quadrotor with X-8 configuration** to provide control during hover and transition and are possibly turned off during forward flight increasing the empty weight of the vehicle as well increasing parasite drag.

A more efficient solution has been developed at University of Maryland, which is a quadrotor biplane MAV [12–14]. The design tries to overcome the mechanical complexity associated with tilting of rotors and wings in tiltrotor or tiltwing type hybrid concepts by making use of the maneuverability of the vehicle for transition. It consists of counter-rotating propellers arranged in a conventional quadrotor configuration, to which are attached two wings in biplane configuration. This design is expected to offer significantly higher control authority and can suc-

cessfully transition from hover to forward flight and back to hover. This design offers better overall performance compared to some of the other options discussed above as it uses same set of propellers for hover and forward flight. However, being powered by battery compromises its industrial usability due to low endurance and range.

The novel design of a quadrotor biplane Vertical Takeoff and Landing (VTOL) UAV proposed and designed in this paper aims at providing solution to several of the challenges discussed above. In this design, a variable pitch H-shaped quadrotor design is combined with two fixed wings attached to the parallel limbs of the quadrotor in biplane configuration similar to that of Hrishikeshavan et al. [12]. The key differences between the two designs are: (1) the use of variable pitch rotors instead of fixed pitch ones, which enables use of internal combustion (IC) engine as power plant, (2) significantly higher endurance, in comparison to battery powered solutions, due to use of fuel engine and (3) use of mechanical transmission to transfer power from engine to the rotors. The vehicle can take-off and land vertically and hover in helicopter mode before transitioning to fixed wing mode to fly with good fuel economy like a fixed wing UAV. The present design is based on the IC engine powered quadrotor work carried out by Abhishek et al. [15].

While, the use of variable pitch propeller and mechanical transmission adds complexity to a simple battery powered design available in literature. The use of variable pitch rotors instead of fixed pitch ones offer the following advantages:

1. Higher control authority and control bandwidth than fixed pitch propellers due to higher rate of change of thrust and ability to generate negative thrust [16]. This would improve maneuverability and gust rejection capability and facilitate transition between different flight modes.
2. The ability to use variable pitch enables the use of fuel engines whereby increasing the endurance dramatically. Gasoline has significantly higher energy density as compared to current Lithium Polymer batteries which are commonly used in UAVs.
3. Different rotor RPMs can be chosen for the rotor during hover and forward flight modes to optimize the rotor power consumption during hover and forward flight.
4. Use of fuel engine reduces turnaround time between flights as refueling is faster than charging batteries.

Design of rotary wing UAVs is well established [17]. However, the design methodology followed for hybrid UAV systems is not fully understood. This paper describes the design, development and flight testing of this novel quadrotor biplane VTOL UAV which has not been studied in literature. The objective is to systematically carry out design of a novel UAV concept, followed by fabrication and flight testing of a scaled proof-of-concept prototype. In Section 2, detailed description of the vehicle is given followed by a discussion of the design methodology in Section 3. For this a physics based modified Blade Element Momentum Theory (BEMT) simulation is developed and validated using experimental data generated for the purpose. To initiate the vehicle design process, first, the proprotor is carefully designed using the above BEMT analysis as discussed in Section 4. Section 5 details the wing design. The conceptual design of the UAV proprotor and wing is followed by selection of power plant, that is described in Section 6. The transmission mechanism required to transfer power from the engine to the rotors is discussed in Section 7. Preliminary structural analysis is presented in Section 8 followed by weight and center of gravity (cg) analysis in Section 9. The avionics and telemetry system used are described in Section 10. In Section 11, the proof-of-concept prototype integration and flight testing is discussed and finally the paper is concluded in Section 12.

2. Vehicle configuration

The proposed design, a quadrotor biplane tailsitter concept, is a novel tailsitter concept comprising of four variable pitch rotors arranged

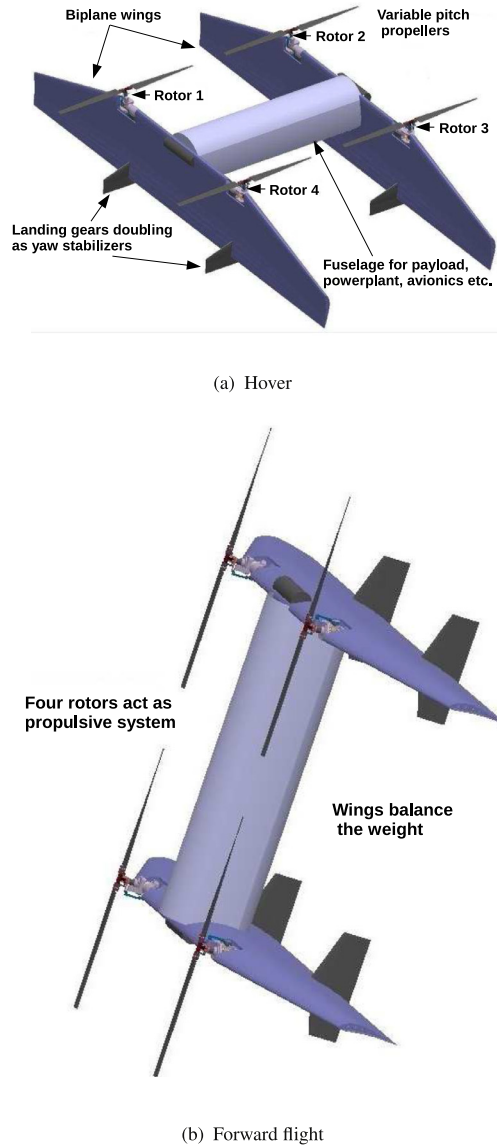


Fig. 1. Hover and forward flight modes of the quadrotor tailsitter UAV prototype.

in a quadrotor like arrangement and driven through a mechanical transmission using a single fuel engine power plant with two fixed wings (in bi-plane configuration) attached to parallel limbs of the quadrotor as shown in Fig. 1. During entire duration of the flight, the wings remain parallel to the propeller axis and hence do not result in any download penalty due to rotor downwash hitting the wings, commonly experienced by tiltrotor type configurations.

The payload can be mounted inside the fuselage of the vehicle which has been designed for this purpose. After gaining safe altitude in hover mode, the rotors would then maneuver and change its attitude from hover mode to forward flight (airplane) mode by generating differential thrust resulting in pitching moment about the center of gravity of the vehicle, required to transition the vehicle to fixed wing mode (forward flight mode) as shown in Fig. 1(b). The VTOL vehicle being designed, attempts to selectively incorporate the advantages offered by both the fixed wing and quadrotor type vehicles, as it can take off and land vertically and hover at a point which is necessary requirement to deliver the payload safely to any destination. During the forward flight mode, it can fly efficiently without any dead weight and attain high speeds to cover large distances required for the last mile delivery.

The primary control of various motions (three translational, roll and pitch motions) in the design is achieved by changing the thrust and torque of different rotors in various combinations during the hover as well as forward flight modes. In the hover mode, the flight control is identical to the control of conventional quadrotor helicopter with fixed pitch, however the mechanism for thrust and torque variation is different for the two. The variation in thrust and torque for the present design is achieved by changing the pitch angle of all the blades in the rotor collectively, as opposed to changing RPM of the rotors.

The roll, pitch and yaw motions in forward flight mode can be controlled by using the same set of controls that are used for flight control during hovering flight. However, it should be noted that, after the vehicle maneuvers into the forward flight mode, the yaw and roll degree of freedom during hovering flight are switched to the roll and yaw degree of freedom respectively. The pitch motion during hover remains the pitch motion during forward flight. In addition, the pitching moment contribution from the wings can be compensated by differential thrust generation by the top and bottom rotors, during forward flight.

The rotor RPM in forward flight mode is reduced from that in the hover mode as the thrust requirements are significantly reduced in forward flight. The entire weight of the vehicle is supported using the thrust from the four rotors during hover, hence the rotors need to operate at a higher RPM as the thrust requirement from each rotor is higher. However, during the forward flight, thrust is required only to overcome the drag of the vehicle which is significantly smaller than the weight of the vehicle. Therefore, the rotor RPM is reduced in forward flight mode to save power. This observation would be elucidated later in text.

Since, the vehicle doesn't have a tail and sits on the biplane wings during take-off and landing, four landing gears shaped like small vertical fins are attached at the trailing edge of the wings as shown in Fig. 1. These vertical fins provide rigid support for the vehicle to land on the ground and also act as vertical fin during forward flight to augment the yaw damping of the vehicle. The sizing of the vertical tail surface has not been considered in the current study and may be taken up in future work.

3. Approach

The design methodology for hybrid UAVs is established by carrying out the design of a hybrid tailsitter UAV with the following mission objectives:

- Payload: 6 kg.
- Range: 32 km.
- Cruising height: 500 m above sea level.
- Cruising speed: 20 m/s.
- Compact vehicle.

These mission objectives have been decided based on the request for proposal of 32nd American Helicopter Society student design competition [18] for a payload delivery UAV.

The complete design and development of the tailsitter vehicle is carried out in various steps. First, the preliminary sizing of the propellers is carried out. Essentially, propellers need to perform optimally in both hover as well as forward flight modes. The propeller sizing and design is carried out by using a modified blade element momentum theory (BEMT) specifically formulated for propellers and propellers. The analysis developed for this purpose is used to study the effect of varying different design parameters such as blade taper, aspect ratio (solidity), twist, radius and tip speed on the rotor performance during hover as well as forward flight. The predictions from the above modified BEMT analysis is first validated using measured thrust and torque data for a variable pitch rotor. A hover test stand with variable pitch rotor head is setup for this purpose and is shown in Fig. 2. The experimental setup consists of a six component load cell mounted on hover test stand with a variable pitch rotor system mounted on top of it.

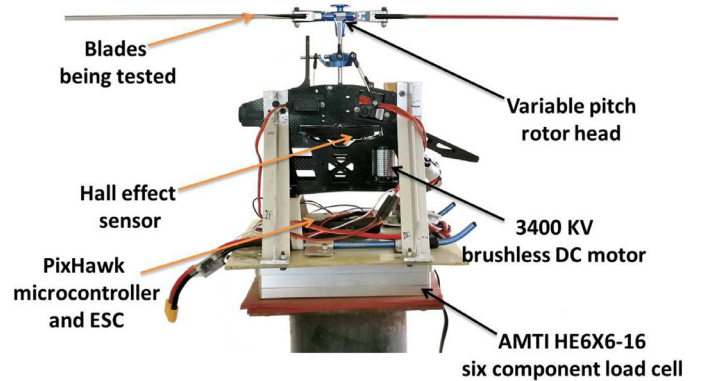


Fig. 2. Experimental setup used for thrust and torque measurements.

Next, the airfoil selection is carried out for the propeller system. Once, the airfoil is chosen, the propellers are sized for radius, chord, twist, taper, number of blades, tip speed etc. based on the performance requirements for both hover and forward flight. The preliminary calculations are carried out based on a nominal weight of approximately 16 kg, which is later on updated as the actual weight of the final design is arrived through detailed weight estimation using CAD drawing.

Next, the aerodynamic design of the biplane wing is carried out to meet the established performance indices. This involves wing loading selection, airfoil selection, planform sizing, material selection. After the rotor and wings have been sized the estimated performance indices allow for the selection of the off-the-shelf power plant. Once, the power plant is selected, the transmission system and the variable pitch mechanisms are designed in detail. After the aerodynamic design is completed, preliminary structural analysis is carried out using commercial-off-the-shelf FEM tools to analyze the factor of safety of critical structural components. The weight estimation and centre of gravity locations are also found out by using CAD software. The estimated weight is used to iterate over the entire design process till a convergence is achieved. Once the design process is completed, the fabrication of the prototype is carried out for a scaled model using appropriate material described later in text.

Finally, a simple proportional-integral-derivative (PID) based attitude controller is developed for the variable pitch quad-rotor system and used to stabilize the vehicle in hovering flight. It is implemented on a PixHawk autopilot board to demonstrate stable hovering flight for the scaled prototype. The control design for transition and forward flight would be carried out in future work.

4. Rotor design

The design of propeller is carried out using modified BEMT with the objective of extracting optimal performance in both hover and forward flight modes. In hover, the propellers provide thrust to support the weight of the vehicle (plus any airframe download) and for this, generous blade area and higher tip speed is desirable. In cruise/forward flight mode, the thrust generated by the rotors has to overcome the aircraft drag only which is a fraction of the vehicle weight. To ensure good propulsive efficiency, the profile losses need to be reduced, which hints at the use of smaller blade area and lower tip speed in cruise mode. This is in contradiction with the requirements for hover.

In this section, the modified BEMT is explained in detail and the subsequent analysis developed for the purpose is validated. The validated analysis is then used to study the influence of various rotor design parameters on hover efficiency and propulsive efficiency.

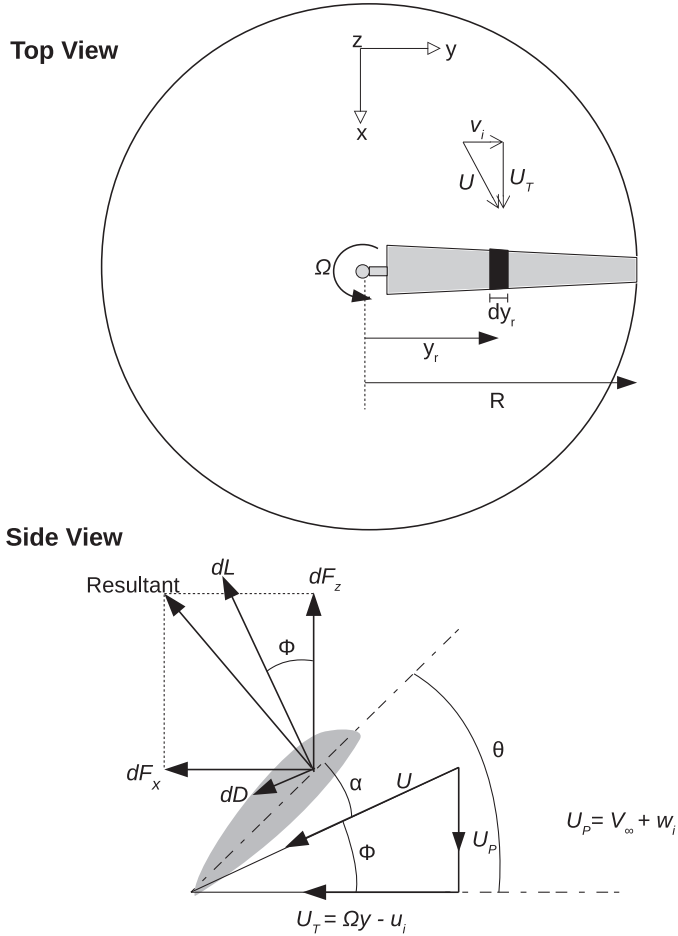


Fig. 3. Velocity components that the blade sections are experiencing.

4.1. Modified blade element momentum theory (BEMT)

The modified blade element momentum theory (BEMT), is described in this section [19]. The modified BEMT differs from the conventional BEMT [20] in the following respects: (1) the small inflow angle assumption is not made, (2) in-plane or swirl velocity component is included in the definition of inflow angle, and (3) Prandtl's tip loss function is modified for large inflow angles.

Fig. 3 shows the schematic of a rotor blade and an element therein. The inflow angle Φ , at each blade section, depends on both the w_i and u_i components of the induced velocity. For a propeller in high advance ratio forward flight, the inflow angles can be large, often exceeding 45° near the blade tips. Therefore, the lift vector on the blade sections may induce flow velocities in the in-plane direction that may be greater than the induced inflow component, hence, both the thrust and torque component are considered for estimating the induced flow-field.

Using the blade element theory, the infinitesimal thrust coefficient generated by a blade element is given by:

$$dC_T = \frac{dT}{\rho A(\Omega R)^2} = \frac{N_b(dL \cos(\Phi) - dD \sin(\Phi))}{\rho A(\Omega R)^2} \quad (1)$$

$$dC_T = \frac{N_b(\frac{1}{2}\rho U^2 c)(C_l \cos(\Phi) - C_d \sin(\Phi))dy_r}{\rho A(\Omega R)^2} = \frac{1}{2}\sigma\sqrt{\xi^2 + \lambda^2}(C_l\xi - C_d\lambda)dr \quad (2)$$

where inflow ratio $\lambda = \frac{(V_\infty + w_i)}{\Omega R}$ and azimuthal flow ratio $\xi = \frac{(\Omega y_r - u_i)}{\Omega R}$

Similarly,

$$dC_P = \frac{dP}{\rho A(\Omega R)^3} = \frac{N_b(dL \sin(\Phi) + dD \cos(\Phi))\Omega y_r}{\rho A(\Omega R)^3} \quad (3)$$

$$dC_P = \frac{1}{2}\sigma\sqrt{\xi^2 + \lambda^2}(C_l\lambda + C_d\xi)rdr \quad (4)$$

The elemental thrust and power coefficients estimated from Momentum theory for a rotor annulus are given by:

$$dC_T = 4|\lambda|\lambda_i r dr \quad (5)$$

$$dC_P = 4|\lambda|\xi_i r^2 dr \quad (6)$$

where out-of-plane induced velocity, $\lambda_i = \frac{w_i}{\Omega R}$ and in-plane induced velocity, $\xi_i = \frac{u_i}{\Omega R}$

4.1.1. Tip loss effect

It is necessary to account for tip-loss effects because only some of the induced flow originates from momentum conservation, the remaining part is due to the presence of the tip vortices. Goldstein [21] established a method for tip-loss by using the velocity potential of a series of helical vortex sheets in the rotor wake. A simplified version of the Goldstein's result was first developed by Prandtl, who approximated the helical surface as a series of two-dimensional planar sheets that convect at the slipstream velocity, which is a more practical mathematical realization of Goldstein's approach [22].

Prandtl's tip loss factor is given by:

$$F = \frac{2}{\pi} \cos^{-1}[\exp(\frac{N_b}{2r} \frac{r-1}{\sin(\Phi)})] \quad (7)$$

This tip loss factor is incorporated in the momentum theory using Kutta–Joukowski theorem

$$dC_T = 4F|\lambda|\lambda_i r dr \quad (8)$$

$$dC_P = 4F|\lambda|\xi_i r^2 dr \quad (9)$$

Because of the inviscid flow assumption, Eq. (8) is only strictly valid when $\Phi = 0^\circ$ and Eq. (9) is only valid when $\Phi = 90^\circ$. At $\Phi = 90^\circ$ for dC_T and $\Phi = 0^\circ$ for dC_P , the tip vortices do not contribute to the induced velocities w_i and u_i . So, in order for these result to match with the expected physical behaviour, the decrease in thrust and power after tip loss i.e $dC_T = 4(1-F)|\lambda|\lambda_i r dr$ and $dC_P = 4(1-F)|\lambda|\xi_i r^2 dr$ should gradually decrease to zero as the angles decrease between the tip vortex axes and the blade force vectors. For incorporating this, the theory is modified as follows.

$$dC_T = 4K_T|\lambda|\lambda_i r dr \quad (10)$$

$$dC_P = 4K_P|\lambda|\xi_i r^2 dr \quad (11)$$

Where $K_T = 1 - (1-F)\cos(\Phi)$ and $K_P = 1 - (1-F)\sin(\Phi)$

The unknown inflow and swirl components can be calculated by equating the thrust and power expressions from blade element and momentum theory.

$$dC_T = 4K_T|\lambda|\lambda_i r dr = \frac{1}{2}\sigma\sqrt{\xi^2 + \lambda^2}(C_l\xi - C_d\lambda)dr \quad (12)$$

$$dC_P = 4K_P|\lambda|\xi_i r^2 dr = \frac{1}{2}\sigma\sqrt{\xi^2 + \lambda^2}(C_l\lambda + C_d\xi)rdr \quad (13)$$

These two equations can be solved simultaneously for λ and ξ using fixed point iteration or any other method. But a different approach, which combines these two equations into a single equation, as shown in [23], and solves for inflow using bracketed bisection method, is used here as it guarantees attainment of solution.

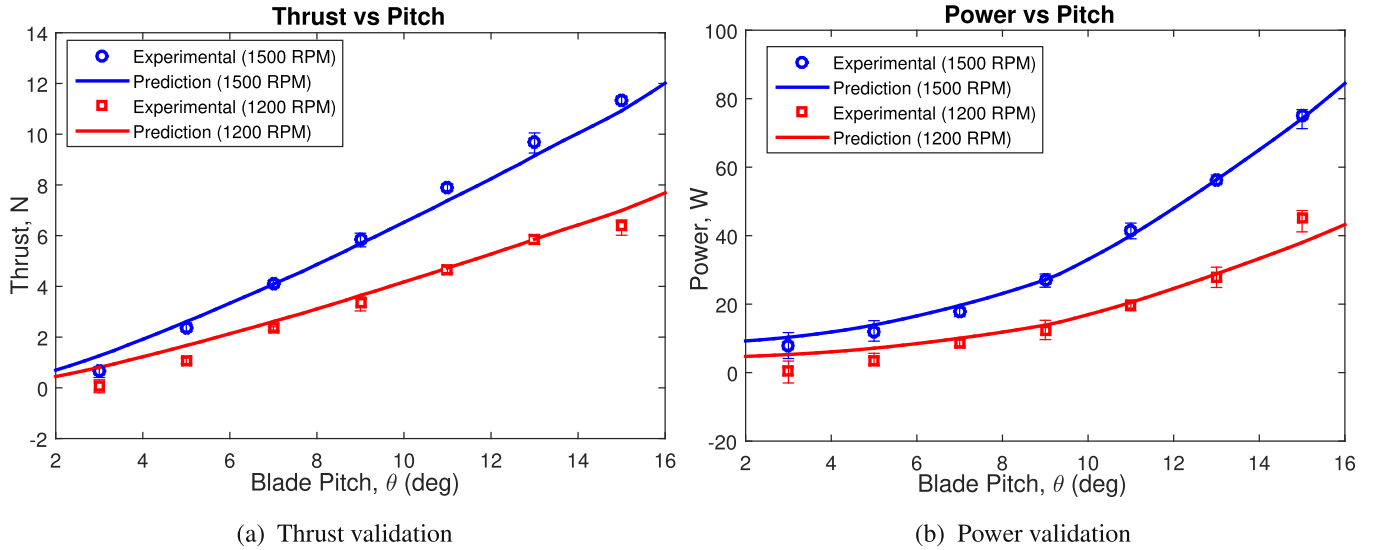


Fig. 4. Experimental validation of present analysis for untwisted helicopter rotor blade with variable collective pitch input.

Replacing $\lambda = \frac{U \sin(\Phi)}{\Omega R}$ and $\xi = \frac{U \cos(\Phi)}{\Omega R}$ and defining $\tan(\gamma) = C_d/C_l$ and putting in Eq. (12), we get,

$$\frac{1}{2} \sigma U^2 C_l \sec(\gamma) (\cos \gamma \cos \Phi - \sin \gamma \sin \Phi) = 4 K_T U \sin(|\Phi|) w_i r \quad (14)$$

We know $w_i = U \sin(\Phi) - V_\infty$

$$\frac{U^2 C_l \sec(\gamma) \cos(\Phi + \gamma)}{8 K_T U \sin(|\Phi|) r} = U \sin(\Phi) - V_\infty \quad (15)$$

Let us define,

$$B_1(\Phi) = \frac{V_\infty}{U} = \sin(\Phi) - \frac{\sigma C_l \sec(\gamma) \cos(\Phi + \gamma)}{8 K_T \sin(|\Phi|) r} \quad (16)$$

Similarly, using Eq. (13) we get,

$$B_2(\Phi) = \frac{\Omega y}{U} = \cos(\Phi) + \frac{\sigma C_l \sec(\gamma) \sin(\Phi + \gamma)}{8 K_P \sin(|\Phi|) r} \quad (17)$$

These two equations can be combined to get a single equation

$$g(\Phi) = [B_1(\Phi)\Omega y - B_2(\Phi)V_\infty] \sin \Phi = 0 \quad (18)$$

$$g(\Phi) = [\Omega y \sin \Phi - V_\infty \cos \Phi] \sin \Phi$$

$$- sgn(\Phi) \frac{\sigma C_l \sec \gamma}{8r} \left[\frac{V_\infty}{K_P} \sin(\Phi + \gamma) + \frac{\Omega y}{K_T} \cos(\Phi + \gamma) \right] = 0 \quad (19)$$

Eq. (19) has Φ as the only unknown and can be solved by using bisection method by having proper range for solution of inflow angle Φ .

4.1.2. Experimental validation of modified BEMT

Modified BEMT is validated with experimental results for an untwisted rectangular rotor with variable pitch and a fixed pitch twisted propeller. The validated analysis is then used for performance predictions of various rotor configurations for design study.

Aerodynamic performance characteristics of a rectangular blade (**radius = 0.3325 m, chord = 3.2 cm, max t/c=12%**) with symmetric airfoil (NACA0012) is measured experimentally and also predicted using BEMT. The experimental and predicted values of thrust and power, using BEMT, for different blade pitch angles for two different rotor RPMs are plotted in Fig. 4. The predictions from the current analysis show satisfactory correlation with the experimental results. The modified BEMT analysis is also validated for a fixed pitch propeller tested by Shastry [24]. The pitch and chord variation along the radius for the propeller (with radius of 14 cm) are approximated by Eq. (20).

$$\theta(y) = 0.0009159y^5 - 0.04202y^4 + 0.742y^3 - 6.151y^2 + 21.24y + 0.1216$$

$$c(y) = -0.001067 * y^3 - 0.02944 * y^2 + 0.6259 * y + 0.5392$$

$$\text{Replacing } \lambda = \frac{U \sin(\Phi)}{\Omega R} \text{ and } \xi = \frac{U \cos(\Phi)}{\Omega R} \text{ and defining } \tan(\gamma) = C_d/C_l \text{ and putting in Eq. (12), we get,} \quad (20)$$

The experimental thrust and power data for the propeller at different rotational speeds is taken from Shastry [24]. As shown in Fig. 5, the thrust and power predicted from the current modified BEMT analysis show excellent correlation with the experimental results. Therefore, the modified BEMT analysis developed can be used for the preliminary design of the propeller with confidence.

4.2. Baseline configuration selection

In the rest of this paper, hover efficiency is assessed either by power loading which is given as $PL = \frac{\text{Thrust}}{\text{Power}}$ or by figure of merit $FM = \frac{\text{ideal power}}{\text{actual power}}$ and propulsive efficiency of the rotor is compared by using propeller efficiency defined as $\eta_p = \frac{C_{T\mu}}{C_p}$. Typically the payload ratio of rotary wing vehicles is around 3–4. For a payload of 6 kg, the assumption of useful load fraction of 0.3 results in approximate gross take-off weight of 20 kg. This requires that each propeller should produce at least 50 N thrust. This information is used to choose the baseline rotor configuration to initiate the design process. A disc loading of 90 N/m^2 (1.88 lb/ft²) is chosen, which has been reported to be reasonable for small UAVs [25]. This results in a radius of approximately 0.42 m for the desired thrust of 50 N. The tip speed is chosen to be 140 m/s which corresponds to Mach number of 0.412 and rotor RPM of 3200. The variation of predicted thrust, using the BEMT analysis validated earlier, for a two bladed rotor with rectangular untwisted blade (selected as baseline) with radius 0.42 m and aspect ratio 10 (chord = 0.042 m) is shown in Fig. 6. The blade airfoil is assumed to be symmetric. It can be observed that the baseline rotor selected is capable of generating 50 N thrust at a pitch angle of 8.5° justifying the choices made. The number of blades is kept at two which is known to be reasonable for small rotors with low disc loading. Typical to propeller design, the rotor blades are given a **preset angle** at the point of its attachment to the hub. This is done to allow for high negative linear twist used in most propellers to prevent the blades from stall under forward flight condition. To begin with the preset angle (θ_{pre}) is set to 0° for the untwisted baseline blades. Therefore, for a given collective pitch input of θ_0 , the blade pitch angle at any spanwise location (r) is given as: $\theta = \theta_0 + \theta_{pre} + \theta_{tw} r$. It is common practice to use the blade preset angle equal to the magnitude of the negative linear twist angle of the blade. This ensures that the blade pitch angle applied directly defines the pitch angle seen by the blade tip.

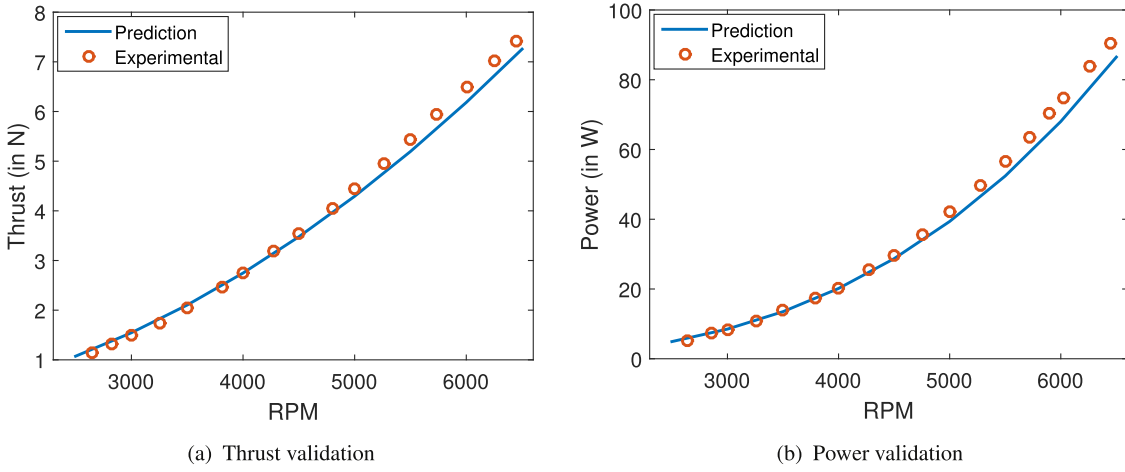


Fig. 5. Experimental Validation of present analysis for a twisted fixed pitch propeller.

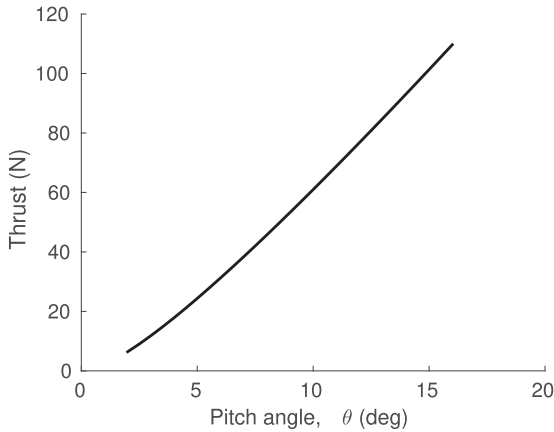


Fig. 6. Predicted thrust vs. blade pitch angle for baseline rotor ($\theta_{tw} = 0^\circ$, $\theta_{pre} = 0^\circ$, $R = .42m$, $RPM = 3200$, $\mathcal{R} = 10$).

4.3. Airfoil selection

Airfoil with high C_l/C_d , high C_{la} , low C_{ma} , and high stall angle are desirable for the proprotor, as such an airfoil would minimize the power requirement of the proprotor. There are several airfoils designed for propellers such as Onera Series HOR 07, 12, 20; EPPLER series E850 to E858; HS1 family HS1404, 30, HS1606, 20 etc. [26] which give satisfactory propulsive efficiency for the propellers. Similarly, airfoils designed for helicopter blade such as EPPLER 360, 361; NPL 9615, 26, 27, 60; Onera series OA206, 09, 12, 13; NASA RC 08,08(N)1, 10-64C, 10(N)1; Sikorsky SC 1094r8, 1095, 1095r8; Boeing-Vertol series VR12 to VR15 etc. [26] are known to perform well for hovering and edge-wise flight of helicopter rotors. For proprotors, airfoils optimized both for hovering as well as high forward speed are needed. Generally, proprotors have multiple airfoils along its span. Because of the inherent high twist that is present in proprotors (reason for which will be discussed later), the root sections operate at very high pitch angles causing the root sections to stall. Therefore, use of thicker airfoil sections with higher stall angles near the proprotor root would maximize hover efficiency. Near the tip, significantly thinner airfoil sections are preferred to reduce the profile power loss, while maximizing figure of merit would require relatively thicker airfoil. Stalhut et al. [19] have reported that for medium-lift tiltrotor, optimizing airfoil section for forward flight has adverse effects on the hover performance. However, optimizing airfoil sections for weighted compromise between hover and forward flight results in only marginal gain in comparison to the results obtained for

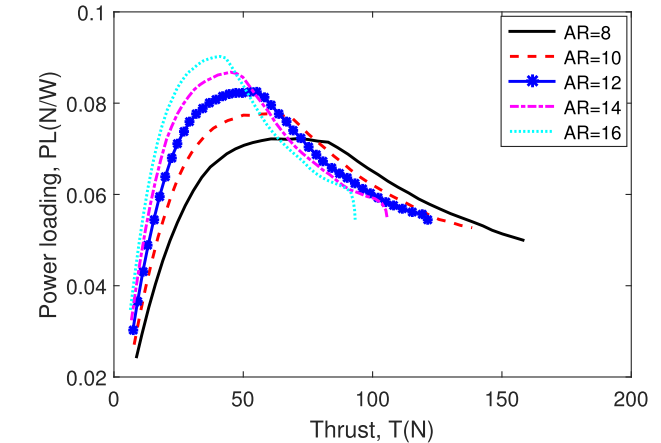


Fig. 7. Effect of aspect ratio (\mathcal{R}) on power loading $\{\theta_{tw} = 0^\circ, \theta_{pre} = 0^\circ, R = .42m, RPM = 3200, \text{no taper}\}$.

purely hover based optimization. Compromised optimization becomes a concern only at high altitudes where higher $C_{l_{max}}$ values are needed to prevent stall near the blade tip. The kind of UAV which is being designed here is not meant to fly at very high altitudes. Therefore, airfoil design and optimization for maximum hover efficiency can give better overall performance without really going into weighted compromised optimization. At the preliminary design stage, which is the focus of the current paper, detailed airfoil optimization is not considered. Instead, a popular helicopter airfoil **SC1095**, the experimental data for which are available in public domain [27,28], is used for proprotor design and analysis.

4.4. Aspect ratio

The effect of changing the aspect ratio of the blade is studied by changing the chord of the blade while keeping the radius constant. Using the modified BEMT analysis, the effect of varying aspect ratio (i.e. rotor solidity for constant radius) during hover is studied as shown in Fig. 7. As expected, an increase in aspect ratio (\mathcal{R}) results in increase in power loading (PL = Thrust/Power) for hover condition. However, reduction of chord length reduces blade area, thereby decreasing the maximum thrust generated by the rotor. For the desired thrust requirement of more than 50 N, \mathcal{R} of 12 appears to be an acceptable compromise between

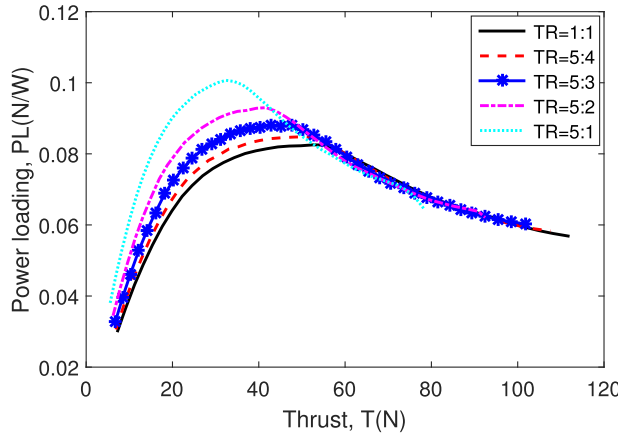


Fig. 8. Effect of taper ratio (TR) on power loading $\{\theta_{iu} = 0^\circ, \theta_{pre} = 0^\circ, R = 42\text{m}, RPM = 3200, AR = 12\}$.

highest power loading and maximum thrust output. Therefore, aspect ratio of 12 is chosen for the current blade design.

4.5. Blade taper

It is known that use of some planform taper for the rotor blade has beneficial effect on hovering rotor performance. This is due to the fact that taper enables the rotor to operate close to maximum C_l/C_d [20]. Therefore, linear taper is incorporated in the BEMT analysis to study its effect on performance of the rotor by using taper ratio, which is defined as $TR = \frac{\text{root chord}}{\text{tip chord}}$. Effect of varying the blade taper ratio, while keeping radius and other parameters same, is shown in Fig. 8. As observed, the power loading (PL) required for hovering flight increases with increasing taper ratio in the range of 20 to 60 N thrust output. However, the maximum thrust output also decreases with increase in taper, due to decrease in the blade area. During the hovering flight condition, the linear taper of 5:3 seems to be a good compromise for generating high thrust (100 N) and moderately high power loading. Hence, the linear taper of 5:3 is chosen for the current design.

4.6. Blade twist

The rotor blade twist is a critical parameter for improving the propotor performance during hover as well as forward flight condition. The effect of varying twist on hover and forward flight performance is studied carefully to bracket the range of values suitable for hover and forward flight. The final value of twist is determined by optimizing the performance within the bracketed range. As discussed earlier, the preset angle at the blade root is set to be equal to the absolute value of the negative rate of twist to ensure that the tip of the blade has same pitch angle for all cases. The variation of predicted power loading with thrust for different values of blade twist is shown in Fig. 9(a). The hover performance, as measured by power loading for the desired thrust of more than 50 N, starts to degrade beyond the twist angle of -15° . Therefore, twist rate greater than -15° is less desirable for achieving good hover efficiency. This is due to the fact that with higher twist the blade has to operate at higher pitch input to generate same value of thrust which causes the inboard region to stall early, which increases the profile power resulting in a decrease in power loading.

On the other hand, during forward flight, the propotor experiences very high inflow angles near the root and the inflow angle decreases along the span. For this reason, a blade with high value of negative blade twist is preferred so that almost every section of the blade operates at optimum lift coefficient. This results in redistribution of the lift and reduces the induced power. The variation of the efficiency of the propotor is shown in Fig. 9(b). The optimum propeller efficiency

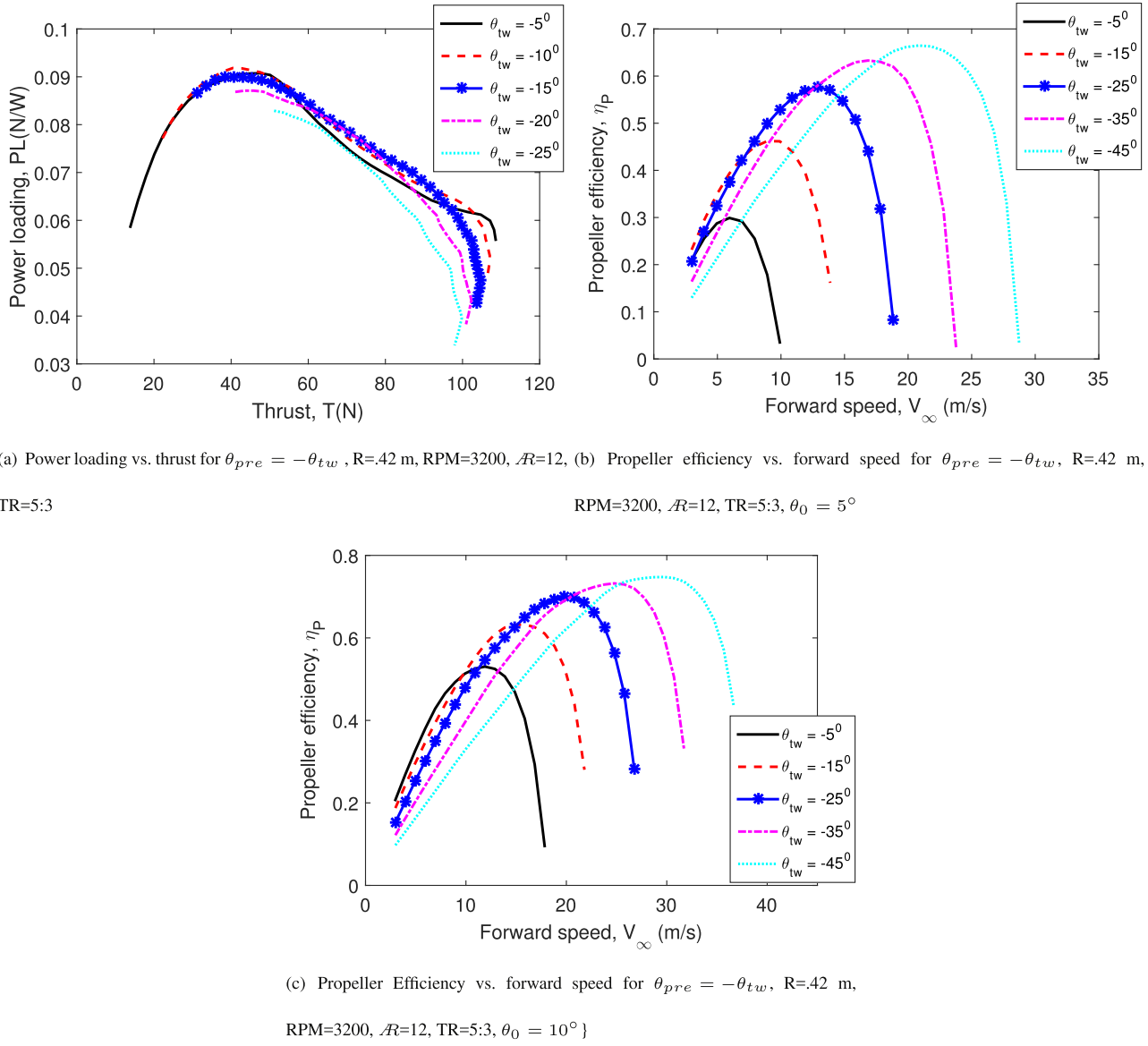
and corresponding speed increase with increase in twist implying that the vehicle can fly faster and with higher efficiency with highly twisted blades. This observation is confirmed for two different blade pitch inputs of 5° and 10° in Fig. 9(b) and (c). It is further observed that at a given twist, an increase in blade pitch input also increases the maximum efficiency and the corresponding speed. Having higher twist also allows optimal performance for wider range of speeds around the desired cruise speed and hence higher twist angle is desirable during forward flight. In summary, a twist between -8° to -15° is desirable for best hover performance while twist between -35° to -45° is desirable for higher propeller efficiency. Because of the conflicting requirements, the blade twist is chosen as a compromise between hover and forward efficiency through manual optimization (discussed later) in which more weightage is given to efficiency in forward flight as the mission profile for the vehicle would require it to spend a significant amount of its mission time in forward flight mode.

4.7. Rotational speed (RPM)

For a given total power available, the rotor torque is inversely proportional to the rotational speed being used. Hence, high rotor speed is desirable as it reduces the weight penalty associated with a heavier transmission system required for higher torque requirements. However, with increase in rotational speed, profile power increases due to compressibility effect and rotor noise also increase. During forward flight, the thrust required to overcome vehicle drag is less than that required to balance the weight of the vehicle during hovering flight. Therefore, the power required during forward flight is significantly less, and it may be advantageous to operate the propotor at reduced RPM during forward flight. Fig. 10 shows the effect of changing RPM on propeller efficiency during forward flight mode. It was established in the previous section that the effect of twist variation for optimal performance lies between -8° to -45° , therefore a nominal value of -30° twist and preset angle of 30° is assumed for the comparison. It is observed that, for the forward speeds in the vicinity of cruise speed (V_{cr}) of 20 m/s, the propotor has highest efficiency for 2000 RPM. The propeller efficiency at 3200 RPM is 0.6079 and that at 2000 RPM is 0.7733 which gives approximately 17% increase in efficiency due to reduction in propotor RPM. Therefore, the operating rotor RPM during forward flight mode is set to 2000 to ensure high propeller efficiency. This is possibly due to reduction in profile power with reduced RPM.

4.8. Optimization

In the previous sections, the aspect ratio, taper ratio and the RPM for the two operational modes of the UAV being designed have been selected through parametric study of the design parameters for the propotor, namely aspect ratio, taper ratio, twist and RPM. The objective of the design process is to minimize the power consumption of the rotors in hover and forward flight. The parametric study carried out in previous sections also revealed that the blade twist has the strongest influence on the rotor performance and the requirements for the hover and forward flight modes are contradictory in nature. Therefore, to manually optimize the power required by the rotor system during entire mission, a simple performance cost function is defined as $\text{cost} = 0.3FM + 0.7\eta_p$. The optimum configuration is identified by giving a manual parameter sweep for blade twist and rotor radius and plotting out the power consumed by the propotor system. The cost function defined uses non-dimensional parameters, namely figure of merit (FM) as an index of hover efficiency and propeller efficiency (η_p) as an index of forward flight efficiency. Based on the typical mission envisioned for the UAV, 30% weightage is given to efficient hovering capability and 70% weightage is given to forward flight performance. This is based on the assumption that the objective of door-to-door package delivery would require the vehicle to spend significant amount of flight time (70% to 80%) in forward flight mode and approximately 20% to 30% of time

**Fig. 9.** Effect of twist on hover and forward flight performance of the proprotor.

in hovering mode to perform precise delivery of payload. It should be noted that figure of merit has its usual meaning which is defined as the ratio of ideal power for the proprotor in hover obtained from momentum theory and the actual power estimated using the modified BEMT. Considering practical constraints based on the design requirements, the optimization is performed for a range of values of radius and twist. The range of values is obtained by performing initial calculations for the given set of requirements during both the flight modes. Formally, the optimization problem can be defined as

$$\left. \begin{array}{l} \text{Maximize } J(R, \theta_{tw}) = \text{cost} = 0.3FM + 0.7\eta_p \\ \text{Subject to } (R, \theta_{tw}) \in S_0 = \{(a, b) \in \mathbb{R}^2, 0.26 \leq a \leq 0.53, \\ -45 \frac{\pi}{180} \leq b \leq -8 \frac{\pi}{180}\} \\ \text{Solution } (R, \theta_{tw}) = \arg \max_{S_0} (J(R, \theta_{tw})) \end{array} \right\} \quad (21)$$

To optimize the performance, the blade twist angle is varied from -45° to -8° (with an interval of 1°) and rotor radius is varied from 0.26 m to 0.53 m (with an interval of 0.01 m) and the figure of merit, propeller efficiency and combined performance cost function are plotted as shown in Fig. 11. Fig. 11(a) and (b) reiterate the contradictory nature of the requirements for optimal hover and forward flight performance.

Table 1
Proprotor design parameters.

Parameter	Value
Aspect ratio	12
Blade taper ratio	5:3
Blade radius	0.38 m
Root chord	0.0475 m
Tip chord	0.0285 m
Blade twist	-24°
Blade preset angle	24°
Rotor RPM (hover)	3200
Rotor RPM (forward flight)	2000

Moderate radius and low twist angle seems to give best hover efficiency, while low rotor radius and high twist are desirable for high propeller efficiency. The objective cost function variation is shown in Fig. 11(c) which is a weighted combination of Fig. 11(a) and (b) as defined in Eq. (21). Based on these calculations, an optimal radius of 0.38 m and blade twist of -24° are chosen which closely brackets the maximum of the cost function for the range of speeds considered. Table 1 shows the

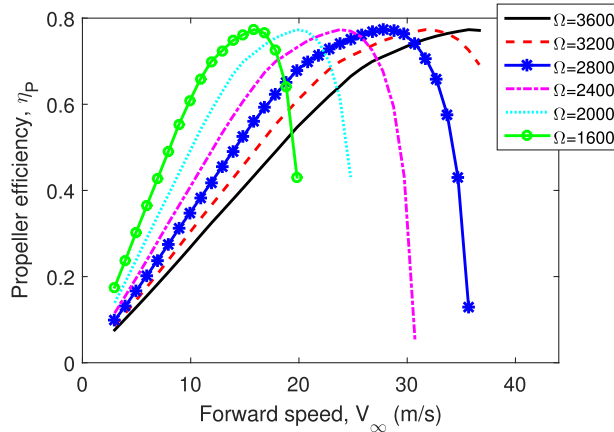


Fig. 10. Effect of RPM on the propeller efficiency $\{\theta_{tw} = -30^\circ, \theta_{pre} = 30^\circ, R = .42m, TR = 5 : 3, \mathcal{R} = 12, \theta_0 = 16^\circ\}$.

5. Wing design

As discussed in [Section 2](#), the proposed vehicle has two wings in biplane configuration. In this section, the detailed design of the wing is discussed along with the justification for selecting the biplane configuration over conventional monoplane design.

5.1. Wing configuration selection

The mission profile of the VTOL UAV being designed requires it to deliver packages in urban canyons with cluttered space. Therefore, the compactness is a desirable feature in the vehicle design. It also ensures easy stowage in warehouses. It is easy to notice that for a given chord, monoplane configuration needs larger span when compared to the biplane design for same wing area. This can be assessed using a simplified analysis based on classical lifting line theory with elliptic lift distribution [\[29\]](#). Consider a monoplane and a biplane, having rectangular planform, with same total wing area and span ratio, β , defined as $\beta = \frac{\text{span of biplane}}{\text{span of monoplane}}$. For a given β and same total wing area, the span and chord of monoplane (b_{w_m}, c_{w_m}) and biplane (b_{w_b}, c_{w_b}) are related as follows

$$\begin{aligned} b_{w_b} &= \beta b_{w_m} \\ c_{w_b} &= \frac{c_{w_m}}{2\beta} \end{aligned} \quad (22)$$

finalized design parameters for the proprotor obtained by optimizing the defined cost function.

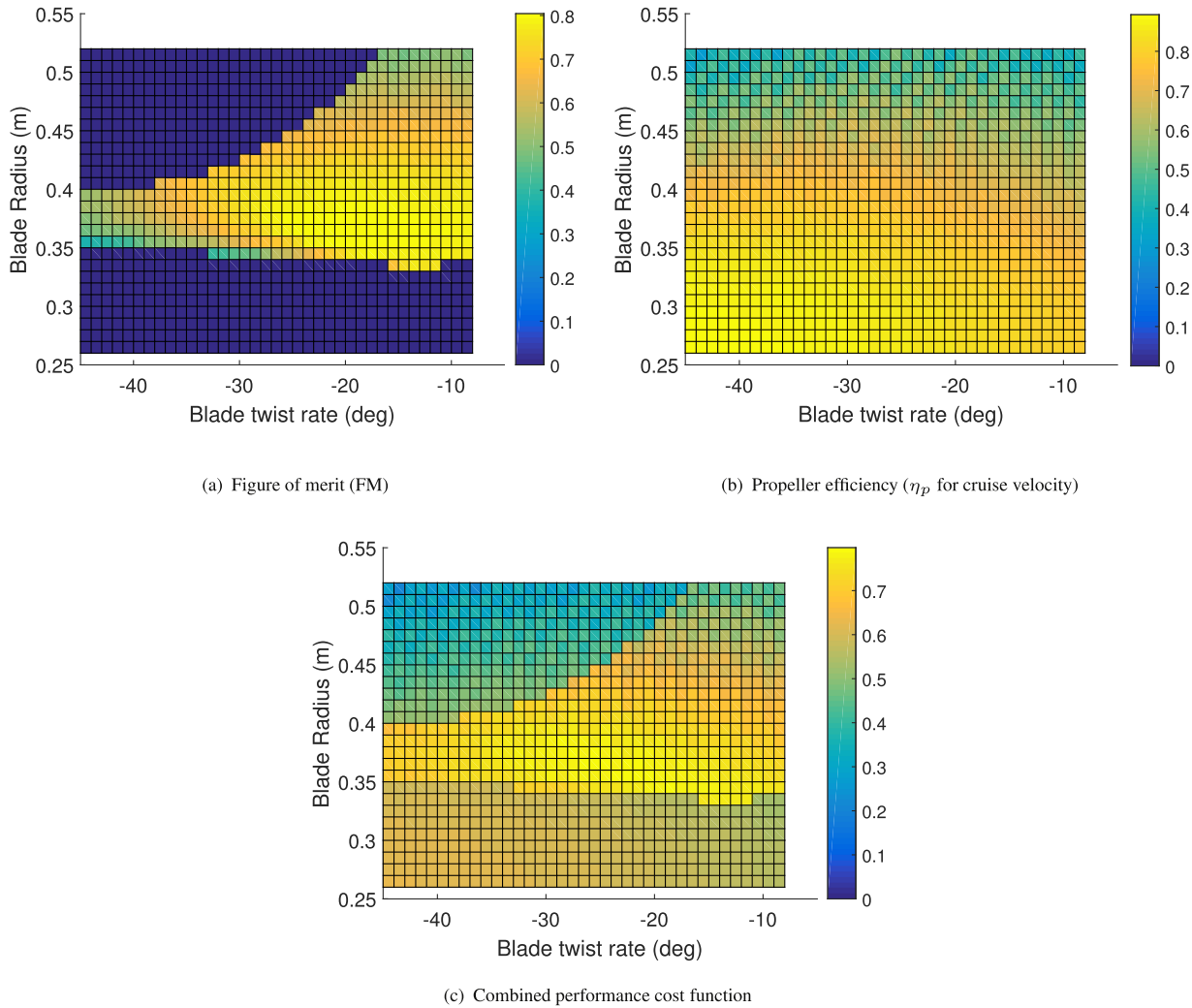


Fig. 11. Manual optimization of UAV performance cost function for radius and twist.

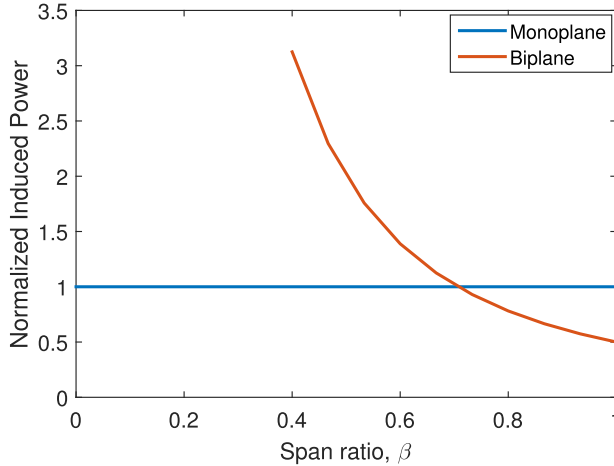


Fig. 12. Comparison of power for monoplane and biplane with same total wing area.

Induced power for monoplane and biplane is calculated using the following equation,

$$P_{ind} = \frac{1}{2} \rho V_{cr}^3 S_w K C_{L_{cr}}^2 \quad (23)$$

where $K = \frac{1}{\pi(\mathcal{R}_w)e}$ and $\mathcal{R}_w = \frac{b_w}{c_w}$. For simplicity, it is assumed

that wings operate independent of each other in biplane configuration. Fig. 12 shows normalized induced power variation for different span ratios defined above. Normalized induced power is the ratio of induced power for biplane to that for monoplane. From this simple analysis, it is observed that in biplane configuration the span can be reduced by up to 30% of the span in monoplane design with the added benefit of requiring less induced power compared to monoplane case. It is known that biplane configuration makes the vehicle structurally more robust and agile [30]. In the current design, the biplane wing also serves the purpose of landing gear. Because of all these benefits, the choice of biplane configuration is justified. For the preliminary design, it is assumed that both the wings behave independent of each other and each wing contributes towards supporting the half of the vehicle weight. Although in practice because of interference between the two wings, the reduction in induced power, in case of biplane, is less than predicted theoretically. For the same span and same area, the biplane should require 50% less induced power than monoplane. But, due to mutual interference between the wings the reduction in power is around 30% instead of 50% [30]. As shown in [32], biplane wings with separation greater than 1.5 times the chord generates approximately 90% of the lift produced by the monoplane with the same total wing area. Based on this, in the current design approach, wing parameters are initially chosen corresponding to monoplane configuration and the span ratio of 0.8 (see Fig. 12) is used to obtain the corresponding span for biplane design to match the induced power of the monoplane configuration. Once, the span is decided, other wing parameters for biplane configuration are obtained to meet the requirement for wing lift.

5.2. Wing loading

Wing loading $(\frac{W}{S_w})$, defined as the ratio of weight of the vehicle divided by the total wing area, affects stall speed, cruise performance and gust tolerance of the vehicle. Since the proposed vehicle can takeoff and land vertically, the constraints on the wing loading enforced by takeoff and landing distances are not relevant. To choose wing loading, power variation with wing loading is plotted for different aspect ratios as shown in Fig. 13. The power is calculated based on the simplified expression shown in Eq. (24). The calculations are performed based on

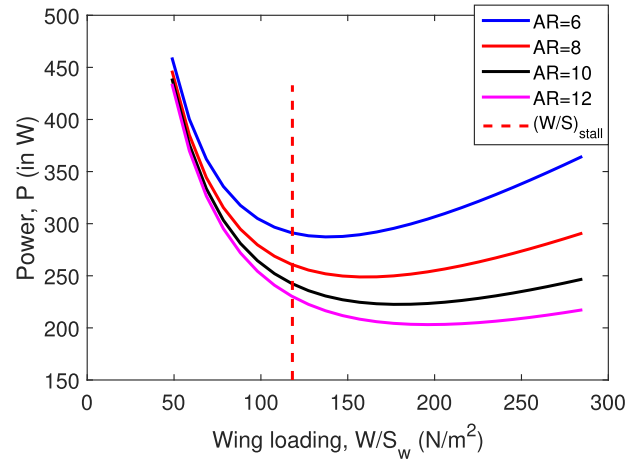


Fig. 13. Power variation with wing loading.

the following typical values for fixed wing UAVs of this category taken from Landolfo [33]: drag coefficient, C_{D0} of 0.025; stall speed, V_{stall} of 12 m/s; oswald efficiency, e of 0.8; maximum lift coefficient, $C_{L_{max}}$ of 1.5.

$$P = \frac{1}{2} \rho V_{cr}^3 C_{D0} \left(\frac{W}{S_w} \right) + 2KW \frac{\left(\frac{W}{S_w} \right)}{\rho V_{cr}} \quad (24)$$

$$\left(\frac{W}{S_w} \right)_{stall} = \frac{1}{2} \rho V_{stall}^2 C_{L_{max}} \quad (25)$$

The critical wing loading corresponding to stall speed, $(\frac{W}{S_w})_{stall}$, calculated using Eq. (25), is also shown in Fig. 13. This value comes out to be around 122 N/m^2 . With larger aspect ratios, the optimum wing loading increases and the power requirement reduces. But, this also increases stall speed and the weight because of the extra structural strength required to support the corresponding high aspect ratio wings. Typically the wing loading for the UAVs of this class, such as ScanEagle, expedition II, Sky Crossbow etc., range from 100 to 170 N/m^2 . Considering all these factors, wing loading of 130 N/m^2 is chosen.

5.3. Airfoil selection

Airfoils with moderate or high camber generate very high lift and typically have high lift to drag ratio. But, high lift comes with high nose down pitching moment [30,31]. For the preliminary analysis, 2D airfoil data available from Landolfo [34] is used for comparing different airfoils. Fig. 14(a)–(c) show airfoil data (C_l vs. C_d , C_l vs. α , C_m vs. α) for the following airfoils commonly used in small UAVs: EPPLER 421, 554, 422; NACA 63; GOE422. EPPLER 421 gives higher lift and lift to drag ratio and also has very high nose-down (negative) pitching moment about quarter chord. The present design is without a tail and the pitching moment from the wing would have to be compensated by use of differential thrust between top and bottom rotor pairs. EPPLER 422 airfoil has second highest lift coefficient among all the airfoils compared and has third lowest nose-down pitching moment and hence is chosen as the primary airfoil for the biplane wings.

5.4. Wing planform

The variation in airfoil characteristics along the span of the wing is largely influenced by wing planform characteristics and so is the performance of the vehicle. An elliptical wing planform has the best lift distribution along the wing but it is difficult to manufacture. A tapered wing has better aerodynamic and structural loads distribution than a rectangular wing. If properly designed, its performance can approach the lift distribution of elliptical wing. However, the small chord near

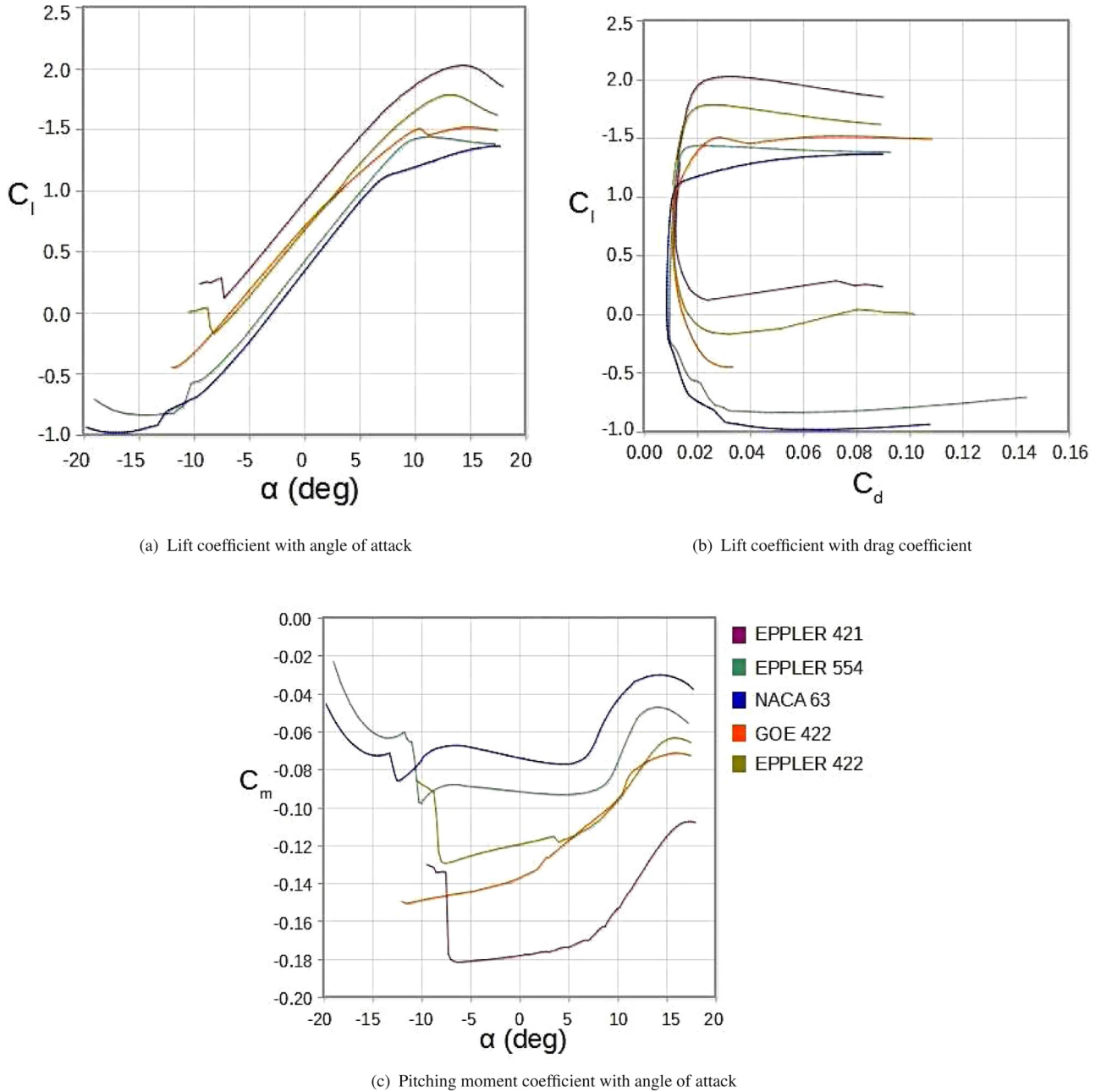


Fig. 14. Comparison of airfoil parameters for different airfoils considered for the wing design.

the tip results in lower Reynolds number and can cause stall [30,31]. Rectangular planform wings do not suffer from this deficiency but have higher drag and worse loads distribution. In the current design the propellers are located at the leading edge of the wing, the wing section up to the location of the propellers is kept rectangular for giving enough space for the transmission system that transfers the power to the rotors. The region of the wing outboard of the rotors is tapered as discussed below. Various aspects of the wing geometry are discussed below.

5.4.1. Aspect ratio

A wing with a high aspect ratio has tips farther apart than an equal area wing with a low aspect ratio. Therefore, the amount of the wing affected by the tip vortex is less for a high aspect ratio and hence experience less loss of lift and increase of drag due to tip effects as compare to a low-aspect-ratio wing of equal area [30]. But with large aspect ratio, the span of the wing will also be larger making vehicle bigger in size.

Typically aspect ratio of 5–8 is used for small aircrafts of this weight class. Therefore, an aspect ratio of 6 is chosen.

5.4.2. Taper

The taper ratio (λ_w) has significant effect on spanwise lift distribution. The spanwise location of center of pressure shifts toward the root with decreased taper ratio thereby decreasing the bending moment about the root. Also the chord at the root increases with decreasing taper ratio for the same wing area providing more structural strength. But highly tapered wing is more prone to tip stall because of the thinner airfoil present at the tip due to decreased chord. Taper ratio of 0.45 is chosen because it gives fairly elliptic lift distribution and good stall characteristics [35].

5.4.3. Sweep

Sweep delays the shock waves and accompanying aerodynamic drag rise because of the compressibility effects near the speed of sound, im-

Table 2
Wing parameters for single wing of the biplane configuration.

Parameter	Value
Wing area	0.754 m ²
Wing Span	2.29 m
Aspect ratio	6.9
Taper	0.45
Root chord	0.39 m
Tip chord	0.176 m
Airfoil	EPPLER 422

proving performance [30,35]. But the vehicle is being designed to fly at low subsonic speeds. Therefore, there is no need for wing sweep.

5.5. Other considerations for wing design

Performance of the biplane largely depends on the gap and stagger between the two wings. Because of the quadrotor configuration attached to both the wings, placing wings at different locations along the wing chordwise direction is not possible, suggesting for zero stagger. Increasing the gap between the wings reduces the interference between the two wings, thereby, making them operate independent of each other and improve the overall aerodynamic efficiency [33,36,37]. As discussed in [32], typically a gap of greater than 1.5 times the chord can give almost 90% of the lift produced by the monoplane with the same total wing area. As discussed earlier, the radius of the rotor blade is 0.38 m so the rotors has to be kept at least 0.76 m apart. For reducing rotor interference, the rotors are kept 1 m apart, thereby constraining the wing separation to be 1 m. Wing gap of 1 m is well above 2.5 times the root chord of the wing, which is 0.39 m, and therefore it is expected that there would be very less interference effect.

The use of dihedral in wings imparts roll stability, but it also reduces the lift generation by the wing and hence has worse aerodynamic performance compared to the wings without dihedral. The use of winglets significantly reduce drag but requires careful designing. However, their impact on wing performance at this scale is less understood and a poor design may increase drag instead of reducing it. Therefore, the use of dihedral and winglets is not considered for the current design. To reduce weight of the wing, it can be fabricated using rohacell foam coated with a thin layer of kevlar composite. The spars made with aluminum alloy cab be used to augment the stiffness of the wing. The use of foam (having low density compared to metals and composites) results in significant reduction in weight of the wing, while coating of kevlar composite layer adds adequate stiffness and rigidity in bending and torsion to the wing.

After having established the wing loading, aspect ratio, and taper ratio etc., dimensions of the wing for monoplane configuration are determined. These parameters are scaled, as discussed above, to obtain parameters for a wing in biplane configuration and are shown in Table 2.

6. Power plant

With the design parameters chosen above, the the power required for the hovering flight is approximately 1.93 hp and 0.7 hp for forward flight condition. Thus, the forward flight mode consumes 64% less power than the hover mode highlighting the advantage of the proposed configuration. To account for the mechanical losses and aerodynamic losses not modeled in the present analysis, an extra 10% power is added to the above estimate, making the desired power output from the engine to be 2.13 hp for hover. To improve endurance, as discussed earlier, gasoline powered 105HZ helicopter engine manufactured by OS is selected as the power source for the vehicle. Besides, being compact and light weight, 105HZ can provide power required for the UAV to hover and have additional power left to enable typical maneuvers needed for rou-

Table 3
Specifications of 105HZ helicopter engine manufactured by OS.

Parameter	Value
Displacement	1.048 in ³ (17.17 cm ³)
Bore	1.442 in (36.63 mm)
Stroke	1.024 in (26 mm)
Practical rpm	2000–16,500
Output	3.75 hp @ 15000 rpm
Engine weight	596 g

Table 4
Specifications of gears in the transmission.

Parameter	E	M1,M2	S1,S2	B
Diameter (in cm)	2	4	8	3.6
No. of teeth	17	34	68	20
Face width (in cm)	3.6	3.6	3.6	0.8
Module, m (in mm)	1.2	1.2	1.2	1.8
Addendum (in mm)	1.2	1.2	1.2	1.8
Dedendum (in mm)	1.44	1.44	1.44	4.1

tine operation. The specifications of the engine selected are given in Table 3.

7. Transmission and pitch change mechanism

Transmission mechanism is shown in Fig. 15 (a). The entire transmission system that transfers power from engine to a propellers consists of three parts.

- 1) Part 1 (Gearbox): To transmit power from the engine to central shafts, gearbox has been used, shown in Fig. 15(b). The gearbox contains 5 spur gears denoted by E, M1, M2, S1, S2. E is the gear attached to the engine shaft, M1 and M2 are gears in the middle, S1, S2 are gears attached to central shafts transferring power to the rotors. Two stage gearbox design has been adopted here to have a smooth transfer of power from the engine shaft to the central shafts. Power requirement during hover is more and hence this power is going to dictate the gear design. The engine will be operating at about 12,800 RPM during hover and the rotors are to operate at 3200 RPM, which means RPM has to be reduced by a factor of 4. For the two stage gearbox design, the RPM will be reduced to half in first stage and to one forth in second stage. This requires the gears to have gear ratios as - E:M1:M2 = 1 : 2 : 2 and M1:S1:S2 = 1 : 2 : 2. For a preliminary design purpose, based on standard design practices, pressure angle (ϕ_0) of 20°, addendum (a_t) of 1 m and dedendum (d_t) of 1.2 m is chosen for design calculations, where m is module. Diameter and number of teeth are determined considering the space constraints as well as the interference between the teeth using Eq. (26) (refer [38]). Face widths (b_t) are determined using American Gear Manufacturers Association (AGMA) strength equation, Eq. (27).

$$T_1 \geq \frac{2a_t \frac{1}{T_2} P_d}{\sqrt{1 + \frac{1}{T_2}(\frac{1}{T_2} + 2)\sin^2 \phi_0} - 1} \quad (26)$$

$$\sigma_b = \frac{F_t P_d}{b_t Y} K_v K_o K_m K_f \quad (27)$$

here T_1 and T_2 are number of teeth on gear 1 and 2 under consideration. P_d is pitch circle diameter. σ_b is maximum bending stress. F_t is the transmitted load. Y is Lewis factor. K_v, K_o, K_m, K_f factors for dynamic loading, overload, load distribution on the gear, and stress concentration effect respectively. Table 4 lists out all the specifications for the gears in the gearbox.

- 2) Part 2 (Transfer bevel gears): For transferring power from central shafts to respective rotor shafts, there are two transfer bevel gears

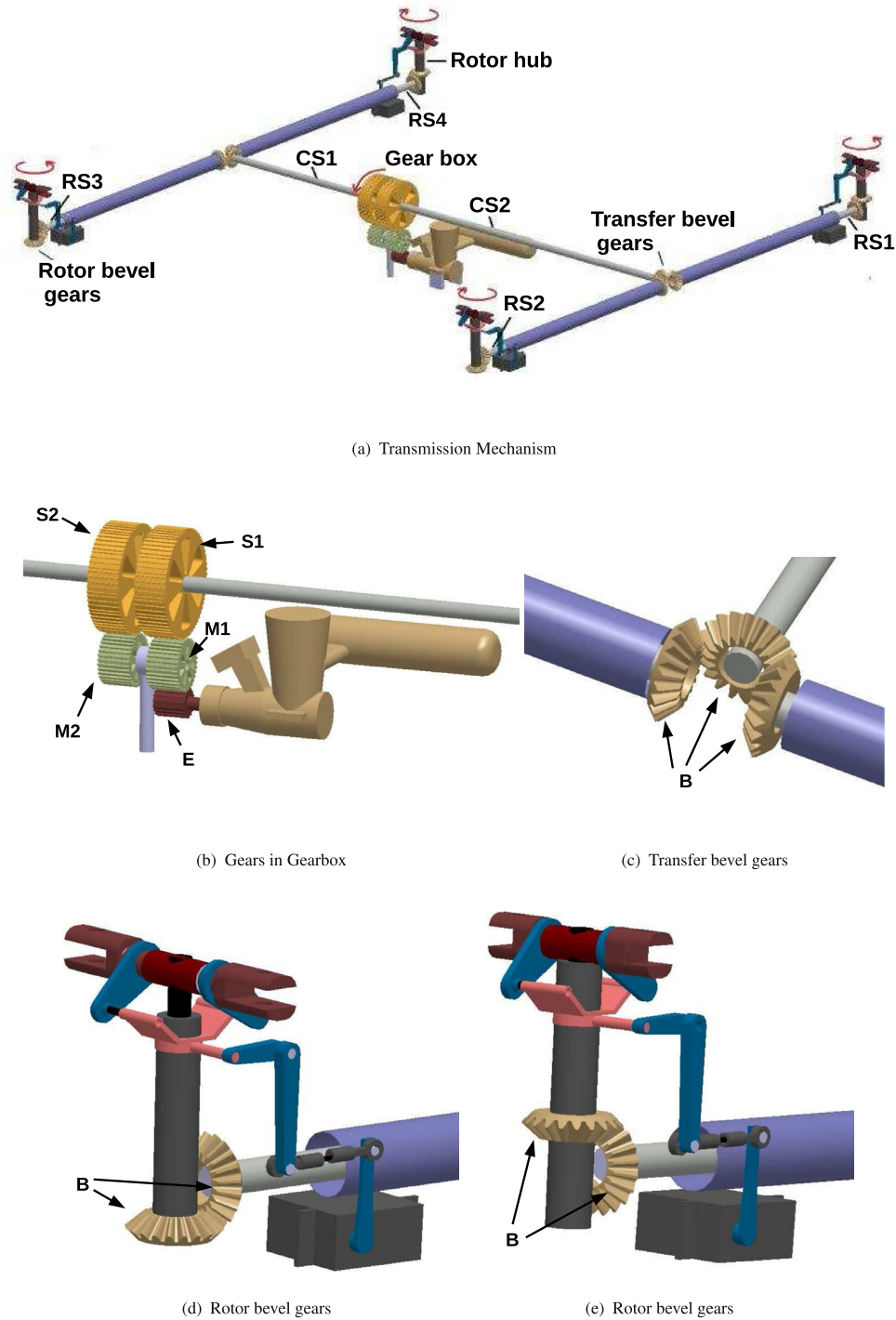


Fig. 15. Schematic of transmission mechanism and gearbox.

- systems which consists of 3 bevel gears (B) each, shown in Fig. 15 (c). One of these three gears is connected to one of the central shafts (CS1, CS2) and transfer power to other two bevel gears kept at 90° and attached to the corresponding rotor shafts (RS1–RS4). All of these three gears are identical, or in other words have gear ratio of 1:1, as the rotational speed being transferred is same.
- 3) Part 3 (Rotor bevel gears): For every rotor, there are two identical bevel gears kept at 90° to transfer power from rotor shafts to the rotor hub, shown in Fig. 15 (d) and (e). The position of the bevel gear attached to rotor hub is such that the adjacent rotors rotate

in opposite direction while diagonally opposite rotors rotate in the same direction.

Fig. 16 shows pitch changing mechanism in detail. The pitch of the blade is changed by moving swashplate, having only heave degree of freedom, up or down by using a servo motor mounted for each rotor on the shaft joining the rotors. For example, as the servo arm is rotated anticlockwise the L-arm rotates clockwise which pushes the swashplate in upward direction which increases the pitch of the anticlockwise rotating blades connected to the swashplate.

The rotational speed of the rotors needs to be changed from that during hover to the one required in forward flight. For the current design,

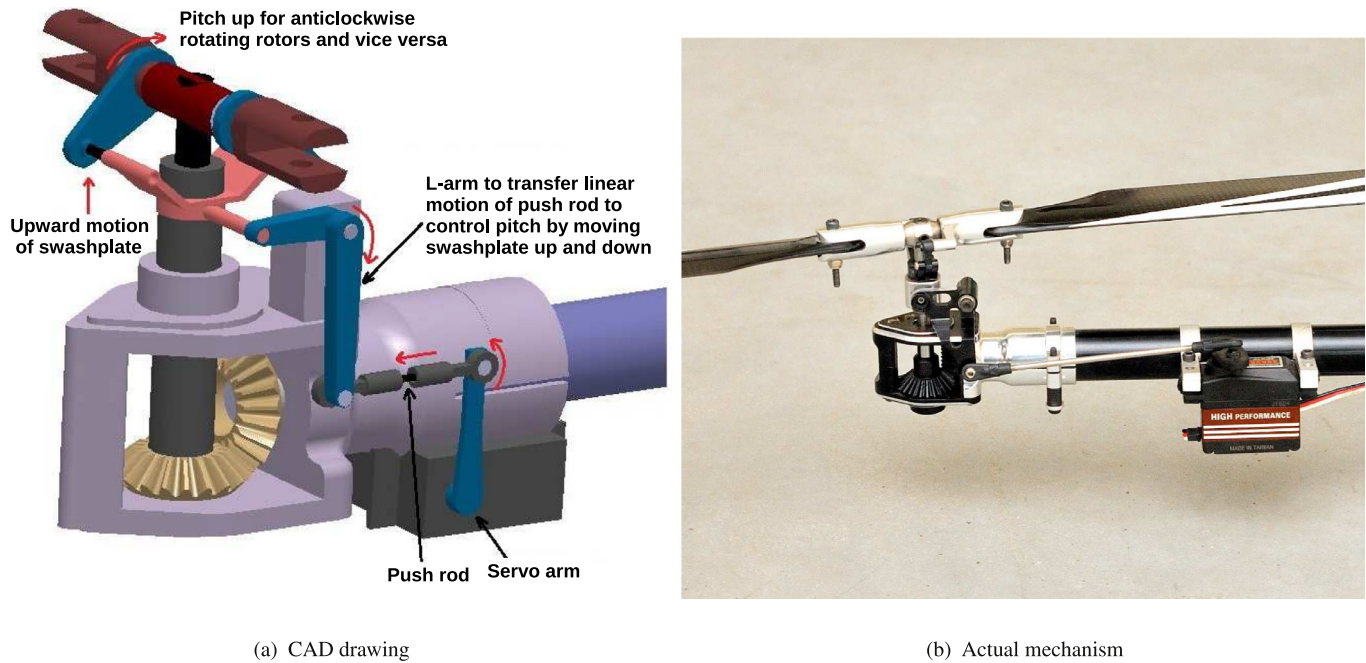


Fig. 16. Schematic of pitch change mechanism.

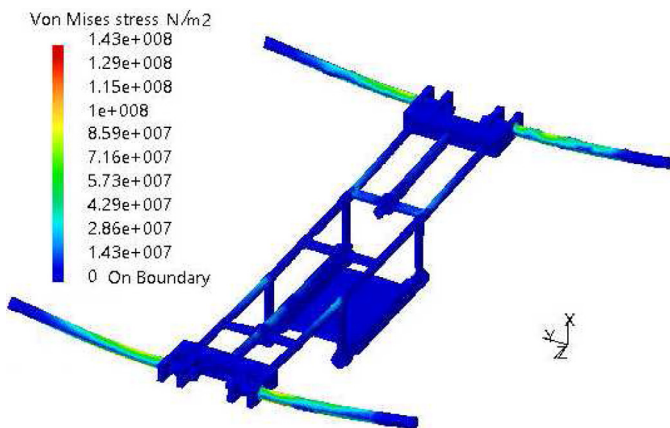


Fig. 17. Structural analysis of quadrotor frame.

this will be achieved by using throttle to change the operating speed of the engine to achieve desired rotational speed and power.

8. Preliminary structural analysis

8.1. Static analysis

To decide upon the dimensions of basic supporting frame and internal wing structure, preliminary structural analysis is performed using CATIA software. First, the parameters are roughly chosen for given loading condition and then static finite element analysis is performed using CATIA software to assess if the structure has adequate strength.

For the main quadrotor frame, the expected rotor thrust during hover condition is applied as point loads at the end of the rotor shaft and the central portion of the frame is fixed to mimic the effect of weight of the vehicle. Fig. 17 shows stress variation over the frame. With the chosen dimensions for frame structure, the minimum factor of safety is estimated to be 1.9 which is above the value required to ensure safe operations. The minimum factor of safety required for UAVs in this category has to be at least 1.5 [39]. Since, the objective is not to optimize the

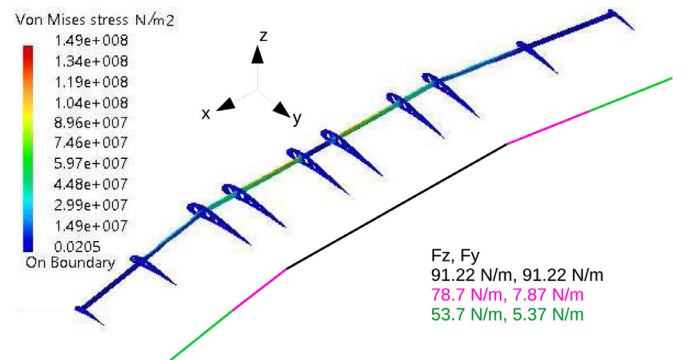


Fig. 18. Structural analysis of wing structure.

structural strength in the preliminary design stage, the chosen dimensions are retained.

For the wing structure, consisting of spars and ribs, the main load carrying members of the wing, distributed loads are applied. Section-wise constant uniformly distributed load is applied having resultant load equal to weight for a single wing. Similarly, drag is also applied, assuming its value to be 10% of the lift. The load distribution and the stress variation for this loading is shown in Fig. 18. The spar has rectangular cross-section of 18 mm × 6 mm. The tip ribs have 2 mm thickness while all other ribs are 3 mm thick. For the given dimensions of spar, the factor of safety is around 1.85 which gives adequate margin for preliminary design.

8.2. Natural frequency analysis

The dynamic analysis of the airframe is an important step to find out the natural frequencies of the airframe to ensure that the design is free from unwanted vibration. The key application of modal analysis is towards mitigation of possibility of resonance in structure due to matching of frequencies of rotors and engine with that of structural components. The vibration analysis of the quadrotor frame is carried out using ANSYS software to find the fundamental natural frequency of the frame

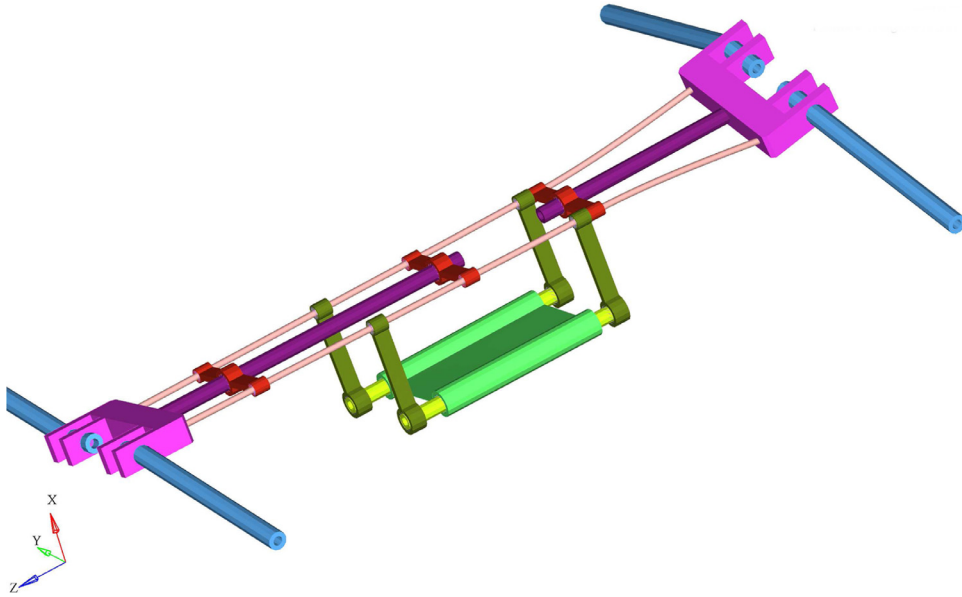


Fig. 19. Mode shape corresponding to the fundamental frequency (19.26 Hz) of the quadrotor frame.

Table 5
Weights of the individual parts.

Component	Weight (Kg)	Quantity	Total weight (Kg)
Wing assembly	1.985	2	3.970
Rotor assembly	0.396	4	1.584
Engine assembly + Gearbox	2.477	1	2.477
Rest frame structure	3.326	1	3.326
Payload	6	1	6
Fuel	1.15	1	1.15
Total weight of the vehicle (Kg)			18.5

at 19.26 Hz and the mode shape corresponding to the fundamental frequency is shown in Fig 19. The rotors operate at 2000 RPM during forward flight and 3200 RPM during hover which corresponds to 33.33 Hz and 53.33 Hz and the engine operates at 15,000 RPM (250 Hz). Therefore, all the forcing frequencies present in the VTOL vehicle are away from the fundamental frequency of the structure and therefore there is no possibility of resonance.

9. Weight estimate and center of gravity location

The detailed drawing of the vehicle is made in CATIA for the dimensions of rotor and wing as designed above and respective material properties are assigned to each and every part. For initial calculations the gross weight of the vehicle was assumed to be 16 kg, but after the initial design and detailed drawing it was realized that the weight of the vehicle without payload is more than 11 kg. Therefore, the calculations were repeated iteratively by refining the initial guess with each iteration until the empty and design weight including payload was in agreement. The estimated weight of various components and the corresponding weight breakdown after the final iteration is shown in Table 5. Center of gravity, because of almost symmetrical design, lies at the center of the quadrotor frame with offset of 15.7 cm towards the trailing edge from leading edge of the wing. The three view drawing of the final design is shown in Fig. 20.

10. Avionics and telemetry

The proposed design is inherently unstable and therefore an on-board autopilot is required to stabilize the vehicle continuously in vari-

ous modes of flight. The open source PixHawk autopilot board with on-board ARM Cortex M4 processor (STM32f407) based micro-controller with a clock speed of 168 MHz is used for stabilization and control for proof-of-concept demonstration of hovering flight discussed in the next section. It has nine degrees-of-freedom IMU (3 axis digital MEMS gyro with range of $\pm 2000^\circ/\text{s}$, 3 axis digital MEMS accelerometer with measuring range of $\pm 16 \text{ g}$ and 3 axis digital MEMS Magnetometer with range of $\pm 12 \text{ Gauss}$), pressure sensor and GPS. The autopilot loop on the PixHawk runs at 200 Hz.

The autopilot software uses open source Mavlink communication protocol for all RTOS inter-process communications as well as ground link telemetry communications related to vehicle health, flight modes, alerts, current position, autopilot arm/disarm status, way-point transfer/switching and sensor calibration. The Mavlink communication protocol also offers cyclic redundancy check (CRC) checksum to reduce data corruption during communication between the ground station and the vehicle. The Linux version of open-source QGroundControl ground station software is used for real-time monitoring and logging of telemetry data. The telemetry module pair operating at 433 MHz is used for all vehicle to ground station communication.

11. Proof-of-concept prototype flight testing

Before, initiating the fabrication of the designed vehicle, a proof-of-concept scaled vehicle is developed based on this design to demonstrate the concept. The baseline variable pitch quadrotor frame is fabricated using the methodology outlined in [15], using commercial-off-the-shelf components (motor, transmission components, servos etc.). In this, the rotors use the same variable pitch mechanism as explained in Section 7 and are powered using a single brushless DC motor through a power transmission. Power from the motor is transferred to a central shaft through a regular spur gear assembly. The central shaft then transfers power to shafts which are normal to it through bevel gears similar to the transmission mechanism explained in Section 7 except that. The detailed description of the transmission system is available in [15]. The wings fabricated using extruded Polystyrene foam are then attached to the quadrotor frame with the help four aluminum clamps, balsa wood and an adhesive. The PixHawk autopilot board is mounted on the vehicle to enable attitude stabilization for hovering flight. The bare variable pitch quadrotor airframe weighs 1000 g, both the wings combined weigh 160 g (are 1 m long each) and the battery is 250 g

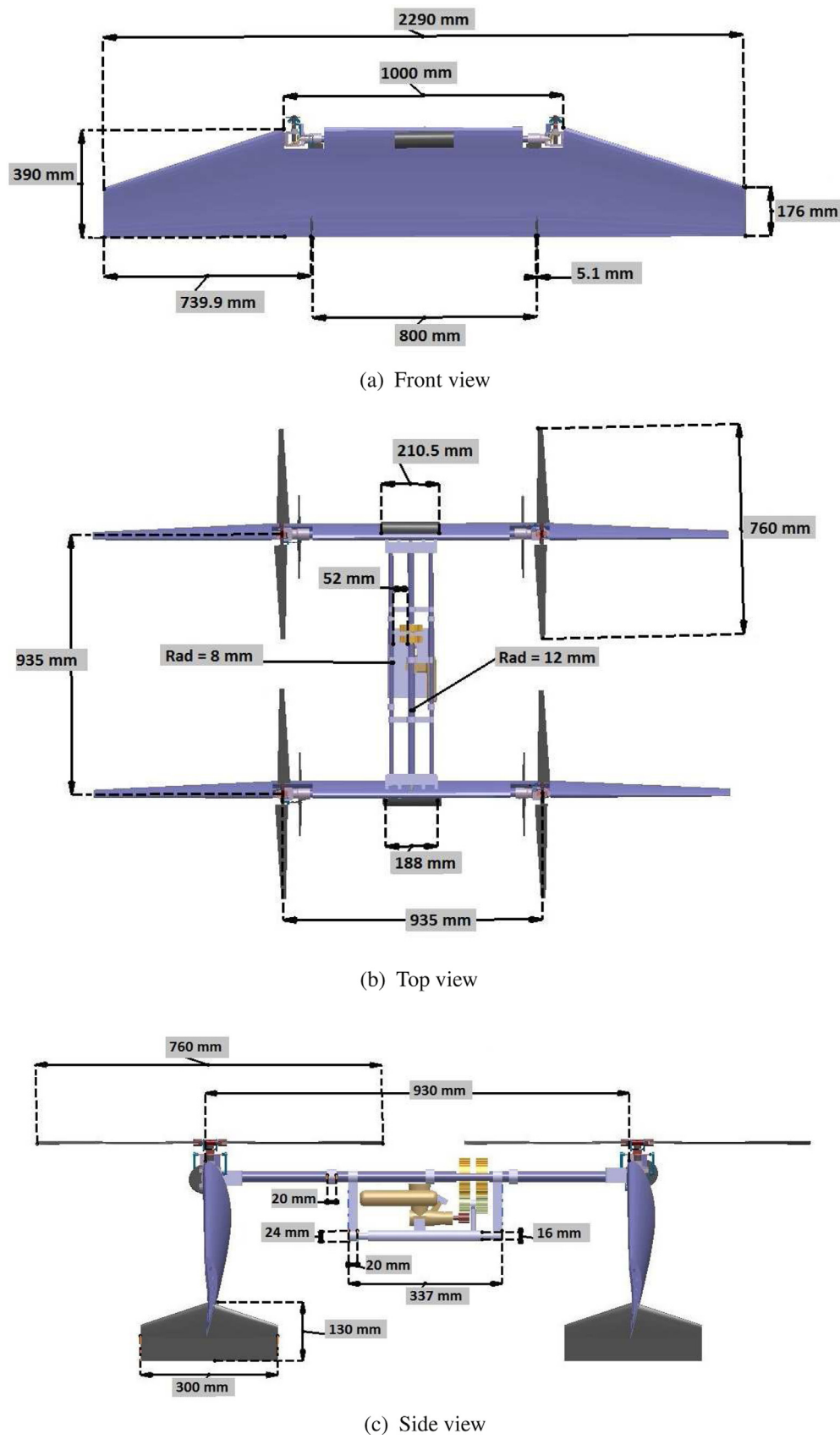


Fig. 20. Three view drawing of designed UAV.



Fig. 21. Variable pitch quadrotor biplane UAV prototype.

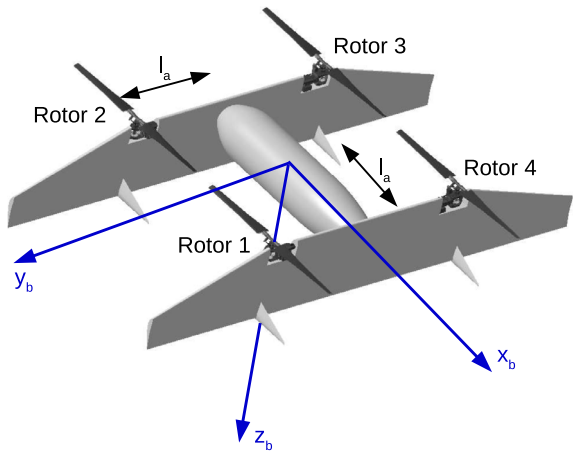


Fig. 22. Coordinate frame.

which amounts to a gross takeoff weight of 1410 g. The vehicle thrust is measured experimentally using a load cell and it is established that

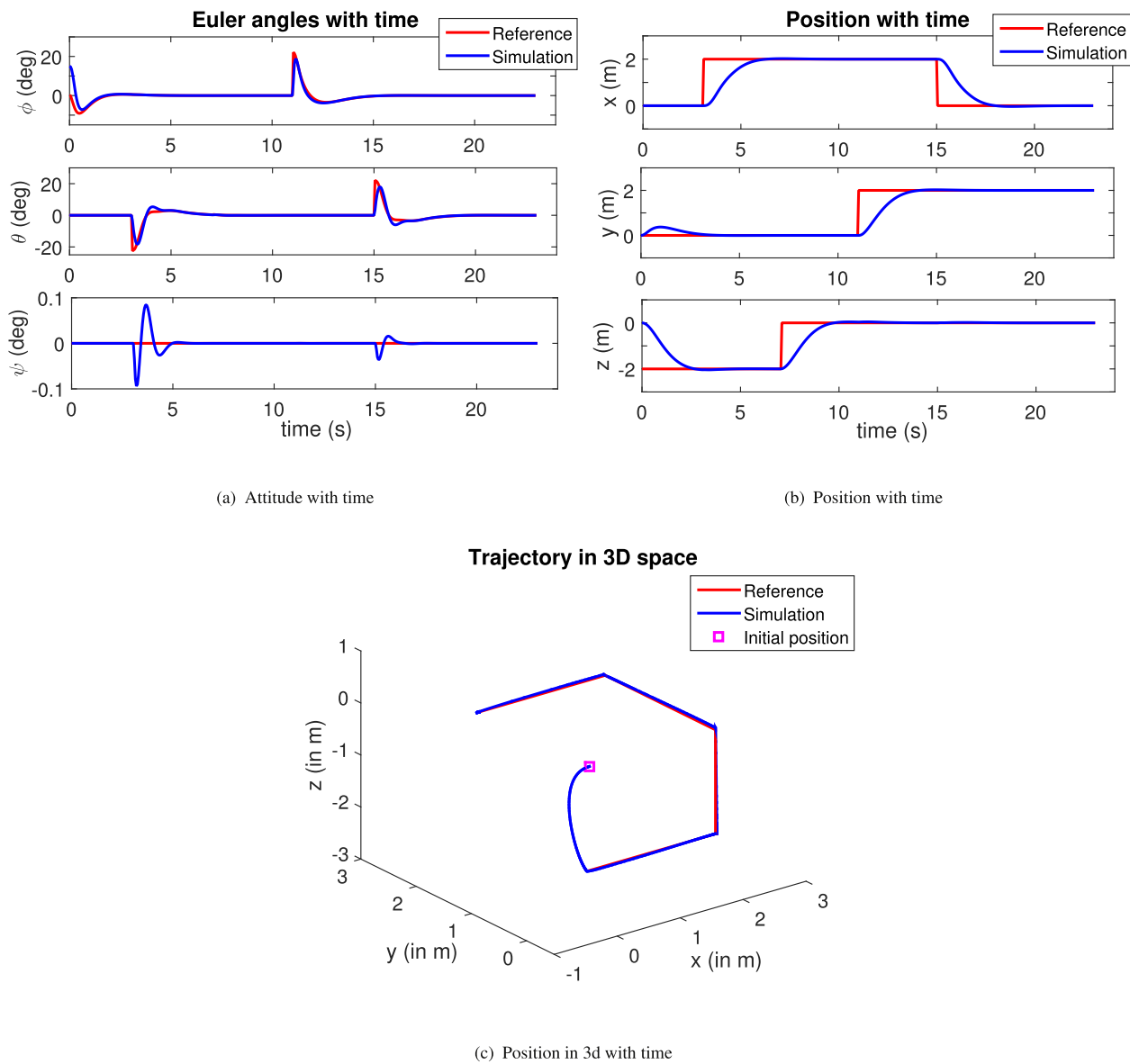


Fig. 23. Simulation for way point tracking.

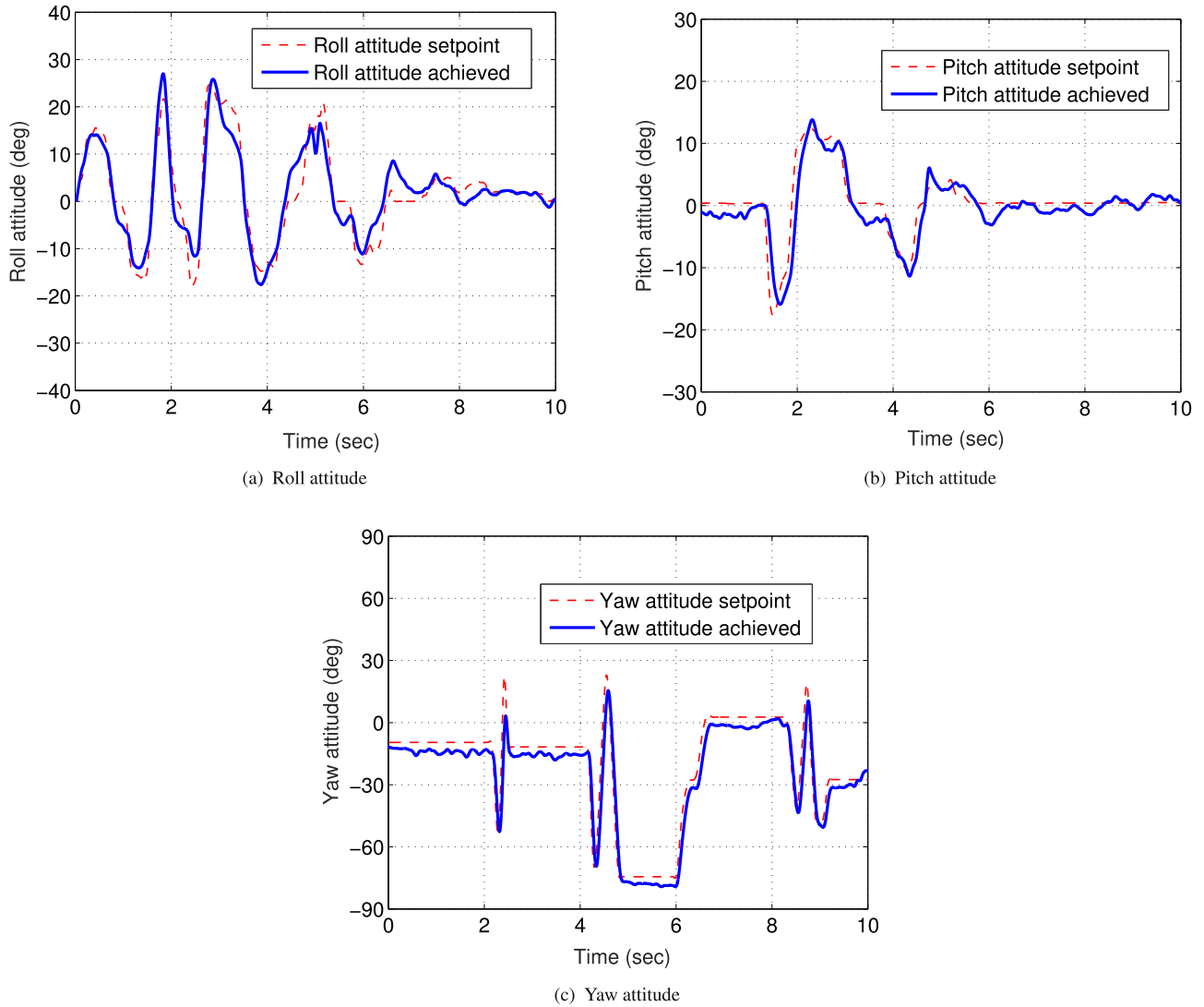


Fig. 24. Experimental validation of controller for attitude tracking of the scaled proof-of-concept prototype.

the prototype vehicle produced a maximum thrust of around 18 N. The assembled quadrotor biplane prototype in hovering flight is shown in Fig. 21. The proof-of-concept demonstration of hovering flight required the implementation of a PID controller for the variable pitch quadrotor system which is discussed below.

11.1. PID control for the variable pitch quadrotor

For attitude stabilization and tracking a simple PID controller is developed and implemented onboard the PixHawk autopilot board. Gupta et al. [40] were first to propose a flight dynamics model for a variable pitch quadrotor UAV which forms the basis for development of the current VTOL UAV. The development of the entire flight envelope autopilot is not the focus of the present paper and would be taken up in future work.

11.1.1. Attitude control

The body fixed frame of reference used to express vehicle angular motion is shown in Fig 22. To achieve the desired orientation $\mathbf{E}_d = [\phi_d \quad \theta_d \quad \psi_d]'$, moments are generated proportional to the Euler angles' errors and their rates using the following expression.

$$\mathbf{M} = -\mathbf{K}_p^a \mathbf{e}_a - \mathbf{K}_i^a \int_0^t \mathbf{e}_a(\tau) d\tau - \mathbf{K}_d^a \dot{\mathbf{e}}_a \quad (28)$$

where $\mathbf{e}_g = \mathbf{E} - \mathbf{E}_d$ and $\mathbf{M} = [l \quad m \quad n]'$

11.1.2. Position control

To track position $\mathbf{r}_d = [x_d \quad y_d \quad z_d]'$, feedback translational accelerations [16], in all the 3 directions, are produced by using the position error and its rate as given below.

$$\ddot{\mathbf{r}}_{fb} = -\mathbf{K}_p^p \mathbf{e}_p - \mathbf{K}_i^p \int_0^t \mathbf{e}_p(\tau) d\tau - \mathbf{K}_d^p \dot{\mathbf{e}}_p \quad (29)$$

where $\mathbf{e}_p = \mathbf{r} - \mathbf{r}_d$. This gives us total accelerations that are required to be applied to the vehicle as follows,

$$\mathbf{a} = M(\ddot{\mathbf{r}}_d + \ddot{\mathbf{r}}_{fb} - \mathbf{g}) \quad (30)$$

where $\mathbf{g} = [0 \quad 0 \quad g]'$; $\mathbf{a} = [a_x \quad a_y \quad a_z]'$. From this accelerations total thrust, desired pitch and roll angles can be calculated as follows [40].

$$\left. \begin{aligned} T &= M\|\mathbf{a}\| \\ \phi_d &= \sin^{-1}(u_x \sin(\psi_d) - u_y \cos(\psi_d)) \\ \theta_d &= \sin^{-1}\left(\frac{u_x \cos(\psi_d) + u_y \sin(\psi_d)}{\cos(\phi_d)}\right) \end{aligned} \right\} \quad (31)$$

where $u_x = \frac{-Ma_x}{T_d}$; $u_y = \frac{-Ma_y}{T_d}$

11.1.3. Control allocation

In case of variable pitch quadrotor, the thrust and torque of each rotor are dependent on the trust coefficients of the rotors which in turn

Table 6
Gains for PID controller.

Parameter	Simulation value	Experimental value
K_p^a	diag([0.61, 0.61, 0.4])	diag([6.5, 6.5, 2.8])
K_i^a	diag([0, 0, 0])	diag([0.05, 0.05, 0.1])
K_d^a	diag([0.2, 0.2, 0.25])	diag([0.15, 0.15, 0.2])
K_p^b	diag([2, 2, 2.2])	diag([0.95, 0.95, 1])
K_i^b	diag([0, 0, 0])	diag([0.02, 0.02, 0.02])
K_d^b	diag([2.2, 2.2, 2.5])	diag([0.09, 0.09, 0.2])

depend on their blade pitch. The total thrust and moments are related to thrust coefficients, obtained using blade element momentum theory, are given below [40].

$$\left. \begin{aligned} T &= K_F(C_{T_1} + C_{T_2} + C_{T_3} + C_{T_4}) \\ l &= K_F l_a(-C_{T_1} - C_{T_2} + C_{T_3} + C_{T_4}) \\ m &= K_F l_a(C_{T_1} - C_{T_2} - C_{T_3} + C_{T_4}) \\ n &= \frac{K_F R}{\sqrt{2}}(-|C_{T_1}|^{\frac{3}{2}} + |C_{T_2}|^{\frac{3}{2}} - |C_{T_3}|^{\frac{3}{2}} + |C_{T_4}|^{\frac{3}{2}}) \end{aligned} \right\} \quad (32)$$

Here K_F is rotor force constant and subscript 1 to 4 denotes the rotor number. Since the yaw moment is non-linearly related to thrust coefficients, for simplicity it is linearized around the hover condition giving expression for yaw moment as in Eq. (33).

$$n = K_F R \sqrt{\frac{C_{T_h}}{2}} (-|C_{T_1}| + |C_{T_2}| - |C_{T_3}| + |C_{T_4}|) \quad (33)$$

where C_{T_h} is thrust coefficient of each rotor during hover. Eq. (32) and 33 are used to obtain thrust coefficients of the each rotor to apply thrust and moments as required from Eqs. (28) and (31). The correlation between thrust coefficients and blade pitch for each rotor is obtained through experiments which is used to generate Pulse Width Modulation (PWM) signals for each of the servo motors that is controlling the pitch of blades in each rotor.

11.1.4. Simulation results

Before the implementation of the controller on the actual vehicle, simulations are carried out for way points tracking. The quadrotor is commanded to track $(x_d, y_d, z_d, \psi_d) = \{(0, 0, -2, 0), (2, 0, -2, 0), (2, 0, 0, 0), (2, 2, 0, 0), (0, 2, 0, 0)\}$. As observed from Fig. 23 (b) and (c), quadrotor tracks the given way points. Similarly, Fig. 23 (c) shows that the required attitude angles generated for position control are also tracked. Table 6 lists out the control parameters used for the simulation and experiments. The inner and outer loops don't use different update frequencies explicitly but rather use appropriately chosen gains for the convergence of the system. The gains for inner loop are chosen sufficiently high such that the inner loop converges to the desired angles required by outer loop quickly enough. The gains used in experiment don't really resemble closely to the gains used in simulation because the dynamics model used in simulation is not that advanced. An enhanced flight dynamics model for the present tailsitter UAV has been developed, validated and used for non-linear control design for full flight envelop operation of the quadrotor tailsitter UAV in [41].

11.1.5. Experimental results

The PID algorithm is implemented on PixHawk autopilot board and used to stabilize and control the prototype during hovering flight. Fig. 24 shows the attitude tracking performance of the prototype vehicle in manual flight. It is observed that the controller tracks roll, pitch and yaw attitude satisfactorily for the vehicle to enable stable hovering flight shown in Fig. 21.

12. Concluding remarks

Conceptual design, of various systems of a novel Quadrotor Biplane VTOL UAV concept and flight test demonstration of proof-of-concept

prototype is presented in this paper. Ingenious use of various technologies such as variable pitch quadrotor, biplane, variable tip speed, and engine as power source makes the vehicle unique in itself at the same time a disruptive technology for today's market. The proposed design is expected to be robust and compact. It is highly maneuverable and capable of performing aggressive maneuvers due to its variable pitch propellers. It has long range due to addition of the biplane wings configuration in its structure and can fly for significantly longer duration due to use of fuel engine. Its landing gears also serve as vertical fins, improving the yaw damping for directional stability. It is designed to land in remote unprepared terrain due to its hovering and VTOL capabilities.

The design of propellers, wings, transmission and structural components is systematically undertaken. The aerodynamic design of the propellers is carried out using modified BEMT. The modified BEMT considers swirl and ignores the small inflow angle assumption. The BEMT predictions are validated against experimental results for helicopter rotor as well as propeller during hover. The propeller design highlights the conflict between the requirements for hover and forward flight. Final propeller design with 24° preset angle and -24° twist is arrived at by giving 70% weightage to forward flight and 30% weightage to hovering flight. The thrust required from the propellers for forward flight, to overcome vehicle drag, is less than that for hovering flight required to support UAV weight. Therefore, a reduction in operating RPM of the propellers from 3200 during hover to 2000 during forward flight results in 27% increase in propeller efficiency. The generation of lift using biplane wings during forward flight mode results in 64% less power consumption, when compared to the quadrotor based hover mode, thereby establishing the benefit of this hybrid concept over conventional quadrotor or helicopter type designs.

Aerodynamic design of the wings is obtained using a typical monoplane wing design approach while optimizing the benefits of the biplane wing configuration. The gears used in transmission mechanism are designed using the standard gear design approach with the help of AGMA equation. The engine is selected as per the power requirement and ensuring high power to weight ratio. Preliminary structural analysis is performed on the base quadrotor frame as well as on the wings using CATIA software. A proof-of-concept vehicle prototype is fabricated and a PID controller is developed to demonstrate stable hovering flight and attitude tracking.

Future work

As a part of future work, first the designed configuration would be fabricated at actual scale. The controller for the entire flight envelope of the vehicle would be implemented and tested, first on the proof-of-concept vehicle and then on the designed prototype. The vehicle would be tested under various flight conditions and its performance would be systematically evaluated.

Acknowledgments

Authors would like to thank Mr. Ramdas Gadekar, a Ph.D. research scholar in Aerospace Engineering department at IIT Kanpur for his valuable assistance during the proof-of-concept prototype flight testing. Authors would also like to thank Ms. Kirti Bhatnagar, Senior Project Associate for her help in CATIA drawings. This research did not receive any specific grant from funding agencies in the public, commercial, or not-for-profit sectors.

References

- [1] Sun J, Li B, Shen L, Chen CK, Wen CY. Dynamic modeling and hardware-in-loop simulation for a tail-sitter unmanned aerial vehicle in hovering flight. In: AIAA Modeling and simulation technologies conference; 2017. p. 0811.
- [2] Wang K, Ke Y, Chen BM. Autonomous reconfigurable hybrid tail-sitter UAV u-lion. Sci China Inf Sci 2017;60(3):033201.

- [3] Seong-Wook C, Youngshin K, Sungho C, Samok K, Jai MK. Development and conversion flight test of a small tiltrotor unmanned aerial vehicle. *J Aircraft* 2010;47(2):730–2.
- [4] Chen C, Zhang J, Zhang D, Shen L. Control and flight test of a tilt-rotor unmanned aerial vehicle. *Int J Adv Robot Syst* 2017;14(1). 1729881416678141.
- [5] Yin Y, Niu H, Liu X. Adaptive neural network sliding mode control for quad tilt rotor aircraftComplexity. 2017.
- [6] Go JI, Park JS, Choi JS. Validation on conceptual design and performance analyses for compound rotocrafts considering lift-offset. *Int J Aeronaut. Space Sci.* 2017;18(1):154–64.
- [7] Flores GR, Escareno J, Lozano R, Salazaret S. Four tilting rotor convertible MAV: modeling, control and real-time hover flight control. *J Intell Robot Syst* 2012;65(1):457–71.
- [8] Cetinsoy E, Dikyar S, Hancer C, Oner KT, Sirimoglu E, Unel M, et al. Design and construction of a novel quad tilt-wing UAV. *Mechatronics* 2012;22(6):723–45.
- [9] Abhishek, Krishna R, Sinha S, Bhowmik J, Das D. Design, development and flight testing of a novel quadrotor convertiplane unmanned air vehicle. 73rd American helicopter society annual forum; 2017.
- [10] BBC News. Article on google tests drone deliveries in project wing trials. 2014. <http://www.bbc.com/news/technology-28964260> [accessed 30.01.2017].
- [11] Amazon prime air; 2016. <https://www.amazon.com/Amazon-Prime-Air/b?node=8037720011> [accessed on 30.01.2017].
- [12] Hrishikeshavan V, Bawek D, Rand O, Chopra I. Development of transition control methodology for a quad rotor-biplane micro air vehicle from hover to forward flight. The AHS international specialists' meeting on unmanned rotorcraft; 2013.
- [13] Hrishikeshavan V, Bogdanowicz C, Chopra I. Design, performance and testing of a quad rotor biplane micro air vehicle for multirole missions. *Int J Micro Air Veh* 2014;6(3):155–74.
- [14] Bogdanowicz C, Hrishikeshavan V, Chopra I. Development of a quad-rotor biplane MAV with enhanced roll control authority in fixed wing mode. 71st American helicopter society annual forum; 2015.
- [15] Abhishek, Gadekar R, Duhoon A, Kothari M, Kadukar S, Rane L, Suryavanshi G. Design, development, and closed-loop flight-testing of a single power plant variable pitch quadrotor unmanned air vehicle; 2017.
- [16] Cutler M, Ure NK, Michini B, How JP. Comparison of fixed and variable pitch actuators for agile quadrotors. In: Proceedings of AIAA Guidance, Navigation, and Control Conference; 2011.
- [17] Cai G, Feng L, Chen BM, Lee TH. Systematic design methodology and construction of UAV helicopters. *Mechatronics* 2012;18(10):545–58. 2008 Pages 545–558, ISSN 0957-4158, <https://doi.org/10.1016/j.mechatronics.2008.05.011>.
- [18] . Request for proposals 2014–2015 of the American helicopter society student design competition; 2014. <https://vtol.org/B2B77560-2C9E-11E4-A41F0050568D0042>.
- [19] Stahlhut CW, Leishman JG. Aerodynamic design optimization of propellers for convertible-rotor concepts. 68th Annual forum of the american helicopter society, Fort Worth, TX; 2012.
- [20] Leishman JG. Blade element theory. In: *Principles of helicopter aerodynamics*. Cambridge: University Press; 2006. p. 115–70. Chapter 2 and 3.
- [21] Goldstein S. On the vortex theory of screw propellers. *Proc. R. Soc.* 1929;123(792):440–65.
- [22] Bradley TH, Mavris D, Moffitt BA, Parkh DE. Validation of vortex propeller theory for UAV design with uncertainty analysis. 46th AIAA Aerospace sciences meeting and exhibit; 2008.
- [23] Winarto H.. BEMT algorithm for the prediction of the performance of arbitrary propellers. 2004. CR CoE-AL 2004-HW3-01, Centre of Expertise in Aerodynamic Loads, Royal Melbourne Institute of Technology.
- [24] Shastry A. A study in dynamics and adaptive control design of quadrotors. Department of Aerospace Engineering, Indian Institute of Technology Kanpur; 2016. Master thesis.
- [25] Hrishikeshavan V, Sirohi J, Tishchenko M, Chopra I. Design and development of a shrouded rotor micro air vehicle with anti torque vanes. *J Am Helicopter Soc* 2011;56(1). 12008–12008.
- [26] On-line depository for airfoil data. UIUC airfoil database. <http://m-selig.ae.illinois.edu/ads.html> [accessed 22.06.2016].
- [27] Davis S.J.. Predesign study for a modern 4-bladed rotor for the RSRA, NASA CR-166155. 1981.
- [28] Bousman W.G.. Aerodynamic characteristics of SC1095 and SC1094 r8 airfoils, NASA TP-2003-212265. 2003.
- [29] Anderson Jr J.D.. Fundamentals of aerodynamics. McGraw-Hill Education; 2010.
- [30] Raymer DP. Aircraft design: a conceptual approach. AIAA: Washington DC; 1992.
- [31] Ming CS. Unmanned air vehicle (UAV) wing design and manufacture. Department of Mechanical Engineering, National University of Singapore; 2010. Bachelor thesis.
- [32] Bogdanowicz CM. Experimental investigation of a quad-rotor biplane micro air vehicle. Department of Aerospace Engineering, University of Maryland; 2015. Master thesis.
- [33] Landolfo G. Aerodynamic and structural design of a small nonplanar wing UAV. Department of Aerospace Engineering, University of Dayton; 2008. Master thesis.
- [34] Online repository for airfoil data. Airfoil tools' airfoil database. <http://m-selig.ae.illinois.edu/ads.html> [accessed 22.06.2016].
- [35] Torenbeek E. Synthesis of subsonic airplane design. Rotterdam, Netherland: Delft University press; 1976.
- [36] Maqsood A, Go TH. Parametric studies and performance analysis of a biplane micro air vehicle. *Int J Aeronaut Space Sci* 2013;14(3):229–36.
- [37] Altman A. Unique stealth unmanned aerial vehicle (UAV) houck aircraft design program. Volume 1: program overview; 2008. Air force research laboratory, Wright-Patterson air force base 45433-7542 AFRL-RB-WP-TR-2008-3170.
- [38] Online article on spur gear design. <http://www.learnengineering.org/2013/02/spur-gear-design.html> [Accessed 22.06.2016].
- [39] Canadian aviation regulations, staff instructions for certification of UAVs, (SI no. 623-001). http://www.tc.gc.ca/eng/civilaviation/standards/general-recavi-uav-4161.html#toc17_0 [Accessed 30.12.2017].
- [40] Gupta N, Kothari M, Abhishek. Flight dynamics and nonlinear control design for variable pitch quadrotors. In: Proceedings of American control conference; 2016. p. 3150–5.
- [41] Swarnkar S, Parwana H, Kothari M, Abhishek. Biplane-quadrotor tail-sitter UAV: flight dynamics and control. *J Guid Control Dyn* 2018;1–19. doi:10.2514/1.G003201.



Vishnu S. Chipade received his B.Tech and M.Tech degree in aerospace engineering from Indian Institute of Technology (IIT) Kanpur, India in 2017. He is currently working as a project engineer at Micro Air Vehicle Laboratory, IIT Kanpur. He is working on adaptive control of variable pitch quadrotor envisioned for package delivery application. His research interests include control and motion planning for Autonomous Unmanned Aerial Systems, rotary wing dynamics.



Abhishek is an assistant professor at the Department of Aerospace Engineering, Indian Institute of Technology Kanpur, India. He did his B.Tech in aerospace engineering from IIT Kharagpur and his M.S. and PhD, also in aerospace engineering, from University of Maryland College Park. His research interests include Rotary Wing Aeromechanics, Helicopter Design, Wind Turbines and Autonomous Unmanned Aerial Systems.



Mangal Kothari received the bachelor of engineering (B.E.) degree in electronics instrument and control engineering from the University of Rajasthan, India, in 2004. He received the Master of Science (M.Sc. Engg.) degree in aerospace engineering from the Indian Institute of Science, Bangalore, India, in 2006 and the Ph.D. degree in control engineering from the University of Leicester, UK, in 2011. He is currently an assistant professor in the Department of Aerospace Engineering, Indian Institute of Technology Kanpur. His research interests include optimal control, nonlinear and adaptive control, flight vehicle guidance and control, nonlinear observer, and motion planning.



Rushikesh R. Chaudhari is an undergraduate student currently pursuing B.Tech- M.Tech dual degree program in Department of Aerospace Engineering at Indian Institute of Technology (IIT) Kanpur, India. He is currently working on development of transition algorithm and performance analysis of proof-of-concept vehicle for Variable Pitch Quadrotor Biplane VTOL UAV.